Energy Conversion and Management 263 (2022) 115687

Contents lists available at ScienceDirect

Energy Conversion and Management

journal homepage: www.elsevier.com/locate/enconman

Constant volume combustion chamber (CVCC) investigations of aerospace F-24 and Jet-A in low-temperature heat release and negative temperature coefficient regions

Valentin Soloiu *, Amanda Weaver, Lily Parker, Austin Brant, Richard Smith III, Marcel Ilie, Gustavo Molina, Cesar Carapia

Department of Mechanical Engineering, Aerospace Laboratories, Georgia Southern University, Statesboro 30458, USA

ARTICLE INFO

Keywords:
CVCC
F24
LTHR
NTCR
Combustion phasing
NVH

ABSTRACT

A study was conducted to determine the characteristics of Low Temperature Heat Release, Derived Cetane Number, and the Vibrations, produced by the combustion of aerospace F24 using Jet-A as a baseline in a Constant Volume Combustion Chamber. The Ignition Delay and Combustion Delay for F-24 were found to be 4.04 ms and 5.71 ms with a DCN resulting at 43.77. Jet-A was found to have a larger DCN of 47 with an ignition delay and combustion delay of 3.35 ms and 5.14 ms. F24 has an extended region of cool flame and releases more of its energy during LTHR than Jet-A, however has a much shorter NTCR than that of Jet-A. From the NVH analysis it was found that there exists a strong correlation between the ID and CD phases and their respective NVH spectrum. It was found that the magnitude of the ringing for Jet-A was 3x higher than that of F24. Meanwhile, the magnitude of vibrations produced by Jet A was approximately 0.5 g greater than those produced by F24′s combustion which correlates well with the higher peak value of AHRR for Jet A and also with higher ringing produced by Jet A compared with F24.

1. Introduction

Combustion engine technology has a wide range of applications, both commercial and noncommercial. The implementation of hydrogen as a clean burning fuel has not yet made the necessary progress to replace conventional petroleum fuels. While there have been developments in electrical aerospace propulsion systems, there is still years of work before a complete transition to electrical power can be made [1]. For both electrical and hydrogen power, there is a current lack of necessary resources to remove the global dependency on fossil fuels.

Jet-A is the petroleum fuel most common in aerospace applications and is defined by the ASTM standard D1655. F24 is modified from its parent fuel, Jet-A, for non-commercial applications using specialized additives for corrosion inhibition, increased lubricity, and dissipation of static charge [11].

In this study, the combustion instabilities, Low-Temperature Heat Release (LTHR) region, and Negative Temperature Coefficient (NTC) regions were investigated for the aerospace fuels Jet-A and F24. These regions have a significant impact on the performance of turbine engines as it has been shown that the lean blowout limit in a gas turbine is directly linked to the LTHR properties through the Derived Cetane Number (DCN) [2]. Furthermore, complex strategies have been implemented in engines to extend the period of LTHR for the purposes of decreasing harmful emissions and increase engine performance [3–10]. In this study, the combustion characteristics of a baseline Jet-A are compared to the fuel F24 for the differences in the low temperature heat release regions and the NVH (ringing oscillations) in a CVCC.

2. Literature review

2.1. Chemical composition of aerospace fuels and the effect of fuel properties

One of the primary factors which contributes to the DCN, autoignition and low temperature heat release characteristics, is the chemical composition of the fuel [12]. The difference between the n-paraffins, *iso*-paraffins, cycloparaffins, naphthalenes, and aromatics as well as the variations between the different branch chain *iso*-paraffins greatly influence the fuel's combustion. A study conducted by Wang et al. [11],

* Corresponding author.
E-mail address: vsoloiu@georgiasouthern.edu (V. Soloiu).

https://doi.org/10.1016/j.enconman.2022.115687
Received 11 January 2022; Received in revised form 24 April 2022; Accepted 26 April 2022

Nomenclature

AHRR	Apparent Heat Release Rate
CD	Combustion Delay
CI	Compression Ignition
CVCC	Constant Volume Combustion Chamber
DCN	Derived Cetane Number
DTA	Differential Thermal Analysis
Dv(x)	Droplet size in μm at x% of the total fuel injected
EOC	End of Combustion
HHV	Higher Heating Value
ID	Ignition Delay
IPK	Iso-paraffinic Kerosene
LHR	Lower Heating Value
LTC	Low Temperature Combustion
LTHR	Low Temperature Heat Release
MFB	Mass Fraction Burned
NTCR	Negative Temperature Coefficient Region
NVH	Noise Vibration Harshness
PRR	Pressure Rise Rate
RI	Ringing Intensity
SMD	Sauter Mean Diameter
SOC	Start of Combustion
SOI	Start of Injection
TAx	Temperature at which x% of fuel's mass is vaporized
TGA	Thermogravimetric Analysis

looked at the variations in the chemical composition of a variety of different conventional and synthetic aviation fuels and their effect on the autoignition behavior of that fuel. This study concluded that the fuels which contained a higher weight percent of linear n-paraffin and light, branched chain *iso*-paraffin hydrocarbons displayed more significant low temperature combustion regions.

A study conducted by Elmalik et al. [13], quantified the role of hydrocarbons on Gas-to-Liquid (GTL) fuel characteristics. The study focused on the primary hydrocarbon building blocks of n-, iso-, and cyclo- paraffins. The researched properties included density, freezing point, and flash point. The study also found that aromatics are of primary concern when looking at the emissions output of the researched fuel. Cyclo-paraffins were found to cause a significant increase in the fuel's density as well as reducing the fuels' heat of combustion at higher concentrations. Different hydrocarbons and other chemical compounds could be determined through hock tube pyrolysis. To quantify the hydrocarbon composition, gas chromatography is one of the more common method to identify the weight of the component hydrocarbons in the fuel [14–18]. From the gas chromatograph in Fig. 1, it is hard to find significant differences between the chemical composition and hydrocarbon distribution between Jet-A and F24. Both Jet-A and F24 contain a complex series of hydrocarbons which can be reflected in the thermophysical properties of each fuel.

Meanwhile, Table 1 based on the work in [9], contains, the percentages of different chemical compounds in F24 and Jet-A. There is a notable higher percentage of olefins and cyclohexanes in F24 over Jet-A.

Olefins produce lower luminosity cool flames with an extended induction period [31] that has also been confirmed in this paper. The

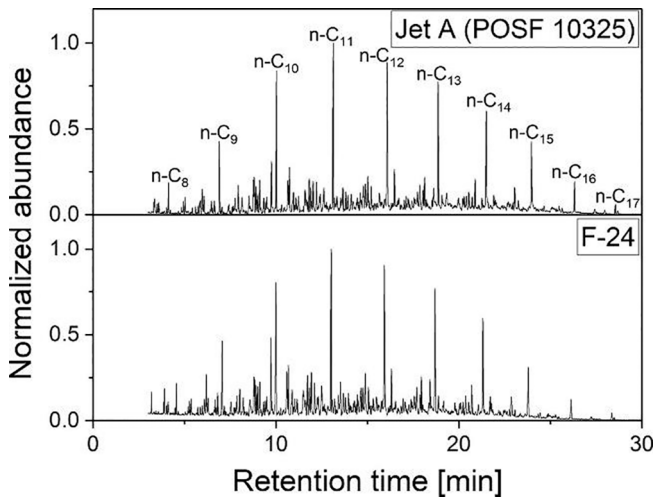

Fig. 1. Gas Chromatography for Jet-A and F24 [19].

Table 1
Hydrocarbon Percentages for Jet-A and F24 [9].

Hydrocarbon Species	F24 (%)	Jet-A (%)
Paraffins	49.57	49.74
Olefins	10.93	6.58
Cyclohexanes	15.5	10.07
Alkylbenzenes	11.47	13.55
Naphthalenes	1.5	2.54
Bicyclics	1.68	1.32
Oxygenates	0.32	2.16
Cymeness	0.79	0.75
Xylenes	0.81	2.67
Alkynes	0.09	0
Other Compounds	0.1	0.5

molecular weight of F24 was found slightly higher than Jet-A at 167.6 g/mol compared to 158.6 g/mol for Jet-A. Additionally, F24 has a higher hydrocarbon ratio of 1.945 as opposed to 1.91 for Jet-A [19]. These differences in the composition of Jet-A and F24 would reflect upon the applications of each fuel. While the general assumption is that these fuels are equivalent, the differences in their applications and behavior in the engine is paramount to providing context for this study.

2.2. *Jet-A and F24, differences between non-commercial and commercial application aerospace fuels*

Jet-A and F24 are both petroleum derived and refined aviation fuels. Jet-A is commonly found in the commercial sector, while F24 is primarily a military fuel. The additives used in F24 are specialized, as outlined in the introduction, and are assumed to create no functional difference between the two fuels [9]. In a study regarding the possible chemical alteration due to the additives in F24 [9], shock tube experiments were performed on the oxidative decomposition of F24. These experiments were conducted at 50 bar and a temperature range of 800 K to 1300 K, and an equivalence ratio of 0.93. That study stated that there were no major functional differences between the combustion of Jet-A and F24, and, as such, used Jet-A as their fuel model for combustion simulation of F24 and Alcohol-to-Jet (ATJ) fuel blends. In this study, the combustion chamber was primed at slightly different parameters based on the ASTM D7668-14.a Testing Standard and the results were also different as presented in the following chapters. Wall temperature and chamber pressure was set to 868.5 K and 20 bar respectively, with an injection pressure and pulse width of 1000 bar and 2.5 ms.

The same additives which make Jet-A into F24 are used to make another military aviation fuel, JP-8. In a study by Kumar et al. [20] the autoignition characteristics of Jet-A and JP-8 were measured with a Rapid Compression Machine (RCM) with variations in the equivalence ratio, pressure, and temperature. JP-8 was determined to have an overall

longer ignition delay time when compared to Jet-A at low temperatures. It was then observed that with the increase in the pressure, the difference in ignition delay times decreased.

A further study by Manigandan et al. [21] researched the impact of blending alternative fuels such as ethanol, pentanol, and two different biofuels on the combustion properties of Jet-A. The study found that the fuel blends with Jet-A changed thrust specific fuel consumption. Thermal efficiency increased with the addition of ethanol as this increased the oxygen content of the reactant species. Through the addition of these compounds to Jet-A, greenhouse gas emissions generated during combustion were decreased. One of the major factors which is changed with the addition of the alcohol fuel is the autoignition characteristics.

2.3. Autoignition characteristics

The autoignition characteristics are primary to the functionality of any engine which are reliant on these characteristics for proper timing, efficiency, and power [22–29]. In a study by Kang et al. [24], the autoignition characteristics of Jet-A surrogates were modeled and validated in both a motored engine and a constant volume combustion chamber. Two different surrogate fuels comprised of different molar percentages of pure component hydrocarbons (n-dodecan, isocetane, methylcyclohexane, decalin, and toluene) were used to replicate aviation Jet-A considering both physical and chemical processes. Observed characteristics were the critical compression ratio and equivalence ratio as well as the % of low temperature heat release. It was found that the different surrogate fuels were comparable to the target fuel with slight trade-offs in the accuracy of different parameters as the researched fuels were altered.

Another study conducted by Cheng et al. [28] studied the autoignition behavior of gasoline-ethanol blends in a rapid compression machine as well as in a homogeneous charge compression ignition engine. This was done to validate experimental results in both a controlled environment and in practical, engine-relevant conditions. The study measured autoignition characteristics through the measurement of ignition delay and primary heat release for blends ranging from 0% to 30% by volume of gasoline and ethanol. Differences between the end of LTHR and the start of high temperature heat release (HTHR) were minimal between the rapid compression machine and the HCCI engine. The study highlights the importance of the characterization of LTHR regions of a fuel for developing new designs and combustion strategies.

2.4. Low-temperature heat release (LTHR) region

The main combustion regions investigated in this study are the Low Temperature Heat Release (LTHR) and Negative Temperature Coefficient (NTC) region. These regions are associated with the formation of cool flames [30]. These cool flames are described as areas in which only a small amount of the reactants combust before being quenched. These flames emit a faint blue light and can occur multiple times during low temperature combustion. These cool flames are then followed by hot flames associated with a high temperature heat release. These two stages of combustion are known as two-stage ignition [31,32]. Derived cetane number is a value which relies on the duration of low temperature burn. Additionally, this region of low temperature combustion plays a role in the emission output [33]. The LTHR region and low temperature ignition (LTI) have been found to have a strong connection to the functional combustion chamber thermodynamic parameters. Factors which affect the LTHR region of a specific fuel include the combustion chamber temperature, pressure, equivalence ratio and the chemical composition of the fuels [33,33–35]. A parametric study by Soloiu et al. [36] on the pressure, temperature, injection pressure and duration in a constant volume combustion chamber to determine the effect of initial thermodynamic conditions on LTI and low temperature combustion with IPK. Internal fuel properties such as the molecular size, structure, bond energy, and functional group can also have an effect on low temperature combustion properties [33]. In a study by Colket et al. [37] the low temperature combustion correlated the lean burnout limit to derived cetane number.

The LTHR region has been linked also to the reduction of harmful greenhouse gas emissions [5]. Multiple strategies based on the low temperature combustion region have been researched and include homogeneous charge compression ignition (HCCI) [4], premixed charge compression ignition (PCCI) [7], and reactivity-controlled compression ignition (RCCI) [38]. Each of these combustion strategies are aimed at reducing the pressure rise rate while increasing the area of low temperature combustion and resulting in emissions' reduction [38–42]. Additionally, the duration of low temperature combustion has been linked to the vibrations caused by combustion [43].

2.5. Combustion instabilities induced noise and vibrations

Noise and vibrations induced by combustion instabilities are a major concern with regard to the performance of the propulsion systems as mentioned also by [44]. Combustion instabilities which cause ringing and other post-combustion shock waves are understood to have also an influence on harmful emissions generation [44–46].

Combustion instabilities can be categorized into static and dynamic instabilities. In gas turbines, static instabilities are identified as flame blowout and flashback. In gas turbines, blowout occurs when the speed of the airflow in the turbine is too large and exceeds flame speed, extinguishing the flame. Flashback is the opposite; this is when the flame speed exceeds the airflow speed and changes the direction of the flow. Both of these conditions are caused by combustion instabilities leading to a reduction in performance and increase in emissions. Acoustic fluctuations of pressure generated by the combustion events cause pressure waves. These fluctuations can be further analyzed by investigating the heat release of the combustion event. In order to keep these fluctuations of pressure to a minimum, different techniques in gas turbines are utilized. These techniques are utilized to lower NO_x emissions while not needing to introduce complex pulse-injection techniques or after treatment systems [47–49].

Dynamic instabilities which occur after the main combustion event, are called ringing events, and can be measured from pressure oscillations. The ringing phenomena is the structural response of the combustion chamber to a very rapid cylinder pressure rise, and ringing includes some combustion events that occur after the main combustion event [50,51]. High levels of ringing cause thermal efficiency losses and damages engine parts, leading to much shorter engine lifespans [52]. In the combustion chamber, the combustion instabilities can be determined from the vibrations of the combustion chamber. These vibrations are measured using highly specialized instrumentation.

This study will focus on the dynamic instabilities caused by the combustion event with a Noise, Vibration, and Harshness (NVH) study, analyzing the unwanted pressure fluctuations occurring after high temperature heat release in the constant volume combustion chamber.

NVH investigations have been conducted on gas turbines to specifically identify the vibrations produced from combustion instabilities. Combustion noise was found to be produced in a frequency range of 200–600 Hz in gas turbines as determined by Dowling et al. [53].

A study conducted by Wissink et al. [54] investigates the frequency composition of pressure oscillations and their relationship to different combustion modes. Experiments were conducted on heavy duty engines in different combustion strategies. It was found that the power contained in resonant frequency modes was profoundly influenced by the heat release event. In a study by Soloiu et al. [55], two aviation fuels, Jet-A and Isoparaffinic Kerosene (IPK), were used to investigate the NVH and emissions produced from a drone jet engine. IPK has a relatively low DCN and an extended ID and CD when compared to Jet-A. Little to no oscillations were discovered in the pressure trace of IPK in the CVCC analysis when compared to Jet-A. The noise, vibrations and emissions were measured in relation to the rpm on the turbojet for both Jet-A and

IPK. It was found that the vibrations produced by combustion instabilities of IPK were significantly lower than of Jet-A. This was then correlated to a drop in the GHG emissions produced by IPK in comparison to Jet-A. Soloiu et al. in [56] found that vibration's signatures of Jet-A, produced by the turbojet main shaft, three exhaust exit fins, twelve compressor blades, and twenty-four turbine blades, the overall frequency produced by each component increased by 1.13%, 1.17%, 1.15%, and 1.01% respectively as the RPM increased to 70,000 RPM. With the increase in operational speed of the turbojet engine from 60,000 to 70,000 RPM, the sound pressure magnitude increased throughout the entire frequency spectrum. The vibrations signatures produced from the combustion of Jet-A in the turbojet engine consisted of diminished magnitudes as the upper regions of operation were reached such as at 25.6 kHz. The greatest magnitudes of vibrations on average occurred at the lower operational range of the turbojet engine which is approximately 0 kHz to 8 kHz.

For this experimentation fuels were evaluated in a Petroleum Analysis Company (PAC) constant volume combustion chamber (CVCC), Brookfield digital viscometer, Shimadzu Thermogravimetric Analysis and Differential Thermal analysis, and a Malvern He-Ne Mie scattering laser to determine the correlation between fluidic fuel properties and combustion characteristics.

This study has been conducted with the goal of bringing a contribution to the understanding of the low-temperature heat release phenomena and negative temperature coefficient region (NTCR) and their correlation between the high temperature heat release region (HTHR), ringing intensity, and induced vibrations due to combustion instabilities. This is a comprehensive and novel study initiated from the debate between the operational similarity of Jet-A and F24 in aerospace turbine engines and the detailed combustion properties. Our study analyzed the fuels' properties and correlated with combustion characteristics and combustion phasing for the same POSF numbers. We found significant differences between both the thermophysical properties and the durations for the LTHR, NTCR, and HTHR of Jet-A and F24.

3. Results and discussion

3.1. Thermophysical properties of researched fuels

The thermophysical properties of the two fuels were determined in order to analyze fluidic properties and combustion phasing and their correlations. The specific properties investigated in this study are the viscosity, Lower Heating Value (LHV), Low Temperature Oxidation through the Thermogravimetric Analysis (TGA) & Differential Thermal Analysis (DTA), Sauter Mean Diameter (SMD), Ignition Delay (ID), Combustion Delay (CD), and Derived Cetane Number (DCN) in a complete and novel consolidation of thermophysical properties as seen in Table 2.

3.2. Energy density determinations: Lower heating value

Determinations of the energy content for the researched fuels were conducted using a Parr 1341 constant volume digital calorimeter as shown in Fig. 2. This instrument is rated by the ANSI for the 0.3% precision class [57,58]. Approximately 500 mg of fuel was placed in a constant volume crucible and was ignited by a fuse wire suspended between two electrodes. The chamber was pressurized with O_2 to 25 atm and submerged into 2 kg of deionized water. A stirring shaft and thermocouple are fixed on the lid of the jacket to get an accurate reading of the change in temperature of the surrounding water to determine the lower heating value for each of the researched fuels. Lower heating value for each of the researched fuels were analyzed and averaged over 5 trials.

Table 2
Thermophysical Properties of Jet-A and F24.

	F-24 (19POSF13664)	**Jet-A** (13POSF10325)
LHV (MJ/kg)	41.85	41.88
DCN*	43.35	46.99
Avg. ID (ms)	4.09	3.35
Avg. CD (ms)	5.79	5.14
Viscosity @ 40℃ (cP)	1.37	1.20
SMD [μm]	18.7	17.59

*DCN determined in PAC CID 510 / All properties determined in the Aerospace Laboratories, Georgia Southern University.

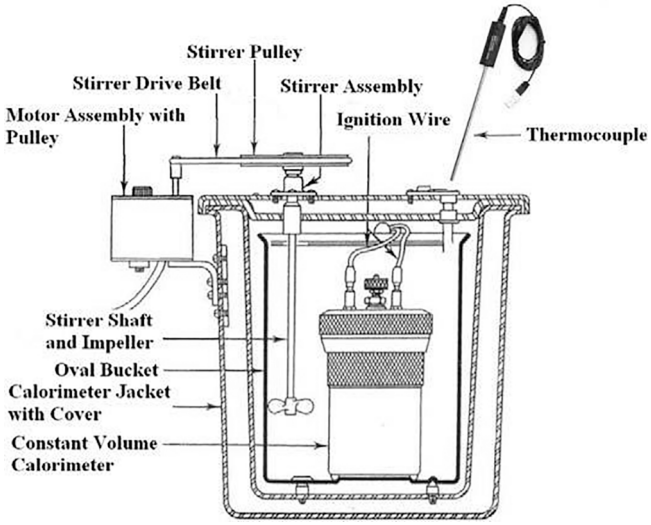

Fig. 2. Parr 1341 Constant Volume Calorimeter [57,58].

The average lower heating value for both fuels are approx. 41.85 MJ/kg, ±0.1%. This lower heating value is dependent on the hydrocarbon ratio of the fuel. A fuel which has a higher hydrocarbon ratio has been correlated to a larger lower heating value [11,59,60].

3.3. Low temperature oxidation and differential thermal analysis

A Shimadzu DTG-60, shown in Fig. 3, was used to perform an investigation of the vaporization rate using Thermogravimetric Analysis (TGA) and the low temperature oxidation using a Differential Thermal Analysis (DTA) for each researched fuel. The chamber was heated from 20 ℃ to 600 ℃ at a rate of 20 ℃ per minute. The furnace was purged

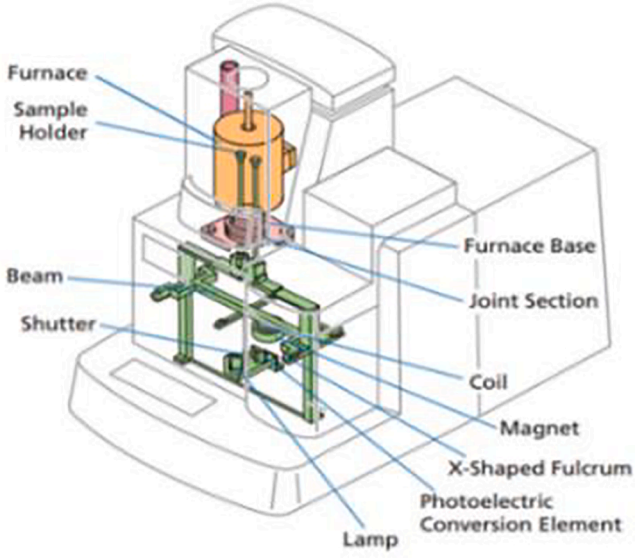

Fig. 3. Shimadzu DTG-60.

with air at a constant airflow rate of 15 mL/min. The TGA assessment is one continuous test with temperature and mass measurements taken at approx. 570 times per minute. The temperature step per measurement was approx. 0.035 °C, and the scale has a sensitivity of 0.01 mg with a variation of ± 1%.

For calibration purposes, an inert alumina powder was used as a baseline for all investigations in the apparatus. The TGA measures the percent reduction in mass of the fuel as the temperature is increased as an indicator of the volatility of the fuel. Additionally, a DTA is conducted to determine the endothermic and exothermic reactions of the fuel with an increase in temperature.

Fig. 4 shows that Jet-A loses mass at a faster rate than F24, and this difference corresponds to a fuel with a higher volatility. Higher volatility is more favorable for combustion because as the fuel vaporizes, it produces a more homogeneous air–fuel mixture at lower temperatures [61,62]. Table 3 shows a representative sample of temperature measurements of the fuel's volatility when 10%, 50%, and 90% of the fuel mass is vaporized. This is then denoted by TA(10), TA(50), and TA(90). F24 started to vaporize at 95 ℃ and was almost completely vaporized by 172 ℃, while Jet-A began vaporization at a lower temperature of 82 ℃, and 90% of the sample was vaporized at 163 ℃. This analysis shows that even though Jet-A and F24 are presumed to have identical properties, a detailed analysis found significant differences.

The DTA of the researched fuels can be seen in Fig. 5. This curve is a representation of the energy that is absorbed and released as the fuel is vaporized and respectively oxidized. A negative slope is an indication of an endothermic process, and a positive slope indicates an exothermic reaction. The slope of the curve relates to the speed at which this energy is absorbed and released. This relates to the TGA analysis in Fig. 4 as the faster energy can be absorbed, the faster the fuel vaporizes.

Fuels with a higher concentration of heavy hydrocarbons are less volatile as those compounds have a generally higher boiling and freezing point. The convex slope corresponds to endothermic reactions, while the concave slopes correspond to the exothermic reactions as seen in Fig. 5. This curve indicates the amount of energy being absorbed as heat energy increases. The results show that the research fuels start releasing energy around TA (90).

It can be seen from this determination that F24 absorbs more energy to vaporize than Jet-A in addition to vaporizing at a slightly higher temperature. Additionally, Jet-A contains a group of heavier hydrocarbons which vaporize at a higher temperature similarly to that of ULSD [43] creating a second endothermic reaction between 300 °C and 500° C. F24, however, has two additional areas of endothermic and exothermic reactions at 250 °C to 350 °C and 425 °C to 550 °C though these reactions have a lower magnitude than the second reaction in Jet-A. In [9] the high temperature oxidations of Jet-A and F24 were determined to have very little difference in the shock tube, but in this paper based on the detailed and precise results in TGA-DTA analysis at temperatures below 600 °C and at the LTHR in CVCC at over 600 °C, there is a significant difference in the low temperature oxidation rates of Jet-A and F24.

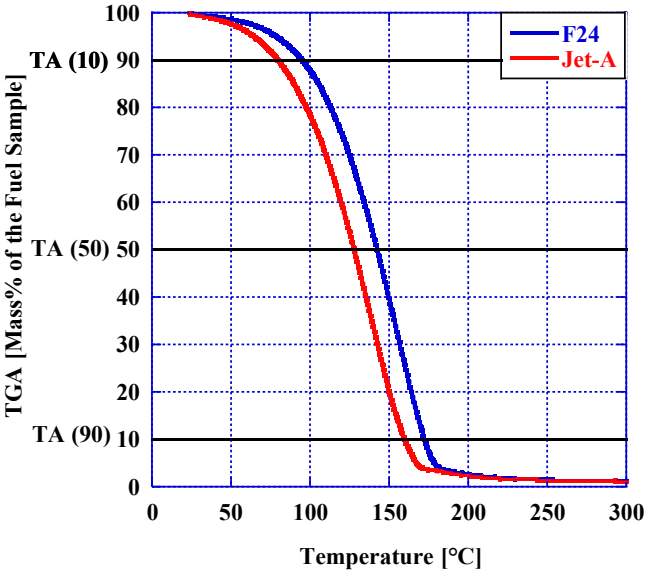

Fig. 4. TGA Analysis of F24 and Jet-A.

Table 3
Thermogravimetric Analysis (TGA).

	F24	Jet-A
TA (10) ℃	94.9	81.67
TA (50) ℃	142.1	129.53
TA (90) ℃	172.1	163.00

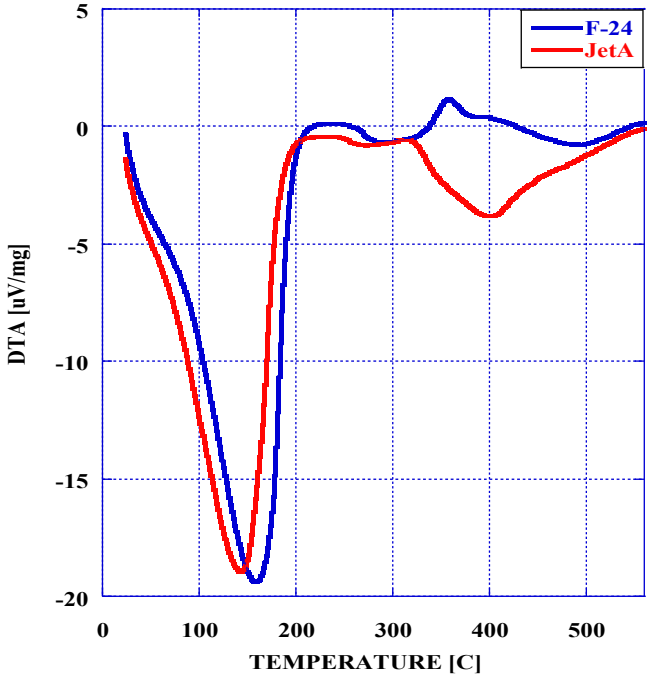

Fig. 5. DTA Analysis of F-24 and Jet-A.

3.4. Spray atomization, droplet distribution and mixture formation investigations with a Mie scattering He-Ne laser system

A Malvern Spraytec He-Ne laser (632.8 nm wavelength) diffraction system, as seen in Fig. 6, was used to determine spray droplet size and distribution for each of the researched fuels. The fuels were injected perpendicularly to the laser beam using a witness single orifice pintle-type Bosch fuel injector positioned 100 mm from the beam with fuel line pressure of 180 bar. 28 of the 36 Spraytec detector sensors (8 to 36) were selected to detect diffracted light signals. Data acquisition was achieved at a rate of 10 kHz starting 0.1 ms before the measurement trigger and ending 5 ms after the trigger. The Fraunhofer diffraction and Mie scattering theories were used to determine Sauter Mean Diameter (SMD) and droplet distribution from the measured diffraction of the laser.

The scattering of un-polarized laser light by a single spherical droplet can be mathematically described by Eq. (1) [63].

$$I(\theta) = \frac{I_0}{2k^2a^2}\left([S_1(\theta)]^2 + [S_2(\theta)]^2\right) \quad (1)$$

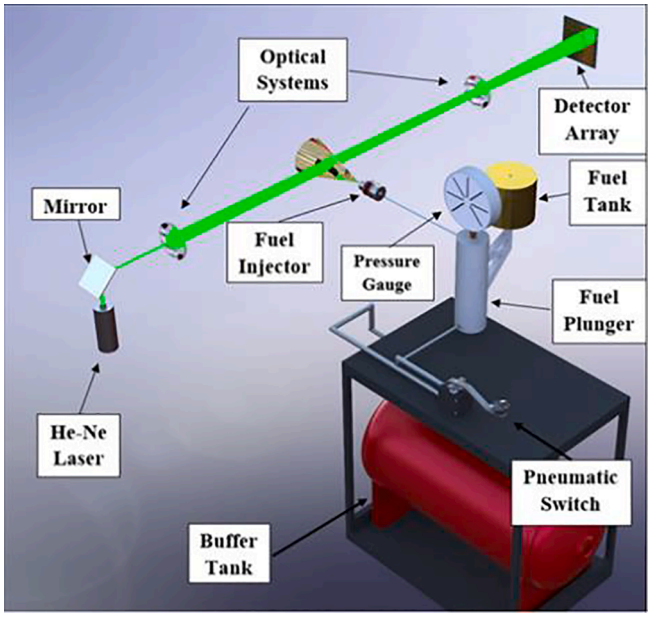

Fig. 6. Mie scattering He-Ne Malvern Spraytec Experimental Apparatus [36].

Where I(θ) is the total scattered intensity as a function of angle θ with respect to the forward direction, I_0 is the illuminating intensity, k is the wavenumber $2\pi/\lambda$, a is the distance from the scatterer to the detector, and S1(θ) and S2(θ) are dimensionless, complex functions describing the change of amplitude in the perpendicular and the parallel polarized light.

The Fraunhofer theory differs from Mie theory in that the optical properties of the particle are not necessary. This allows for the practical application of the theory to be used for the measurement of mixtures of different materials and shapes. The equation for I(θ) simplifies to the following formula, denoted in Eq. (2) [63], with the dimensionless size parameter $\alpha = \pi x/\lambda$, where × represents particle size.

$$I(\theta) = \frac{I_0}{2k^2a^2}\alpha^4\left(\frac{J_1(\alpha\sin(\theta))}{\alpha\sin\theta}\right) \quad (2)$$

SMD, also known as surface area weighted mean, was the sizing method chosen to report the fuel droplet size because of the significant role that surface area plays in atomization, mixing with air, and subsequent combustion.

For F24 and Jet-A, the average frequency at which droplets of specific size classes developed across multiple sprays was characterized by the volume density (%) that each droplet size class represented of the total spray volume. The ten sprays of F24 and Jet-A were also characterized by average SMD measured as the spray developed over time (10,000 measurements per second). A much better understanding of these two spray characteristics can be gained by viewing the graphs presented in Figs. 7 and 8.

The average SMD of Jet-A was found to be 17.59 μm, while F24 was 18.7 μm as seen in Table 4. The droplet distribution of the fuels is denoted by Dv(10), Dv(50), and Dv(90) which corresponds to 10%, 50%, and 90% of the total spray volume respectively. The spray distribution is presented in Table 5.

3.5. Dynamic viscosity determination

An important factor in determining a fuel's fluidic flow and spray atomization characteristics is the fuel's viscosity. Fuels that have a higher viscosity will produce a spray with larger droplets [64,65]. Larger droplets have a smaller surface area to volume ratio leading to slower or even incomplete combustion [60,65,66]. A Brookfield DV-II + Pro rotational viscometer, as shown in Fig. 9, was used to determine the viscosity of each of the researched fuels. The Brookfield DV-II + Pro calculates the viscosity of the fuel by measuring the change in the torque applied to the suspended spindle and shear stress in the fuel. Determinations of the dynamic viscosity of the fuel uses Eq. (3).

$$\eta = \frac{\tau}{\dot{\gamma}} \quad (3)$$

The dynamic viscosity is represented as η in units of Pa^*s, shear stress is measured in N/m^2 represented by τ, and the shear rate is $\dot{\gamma}$ measured in s^{-1}.

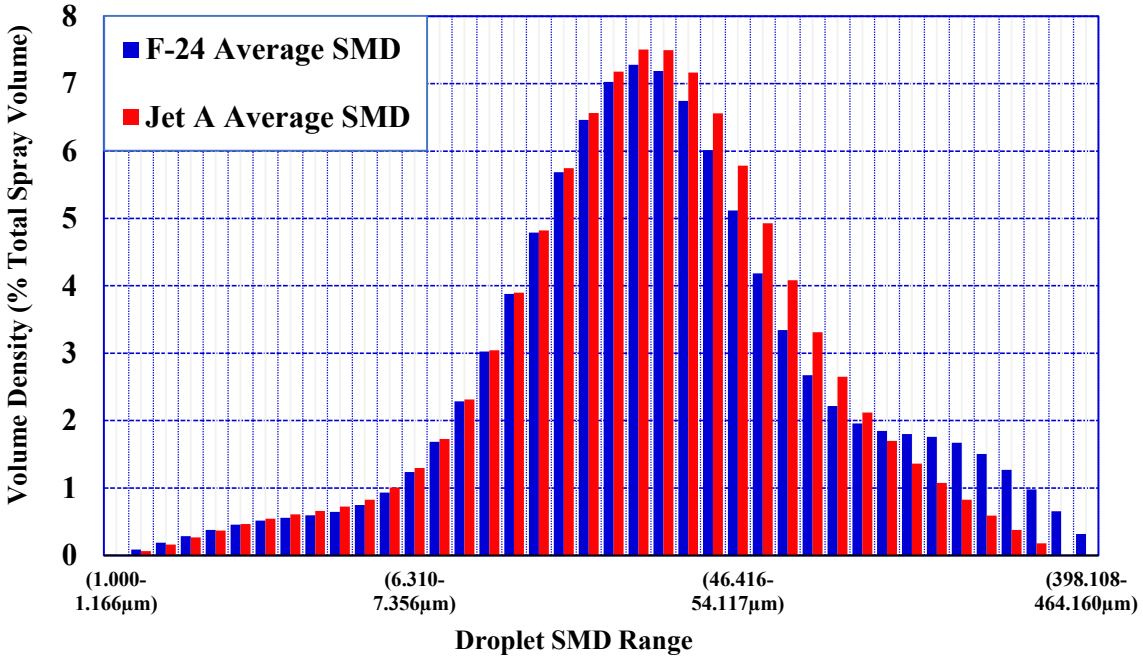

Fig. 7. Spray Droplet Distribution.

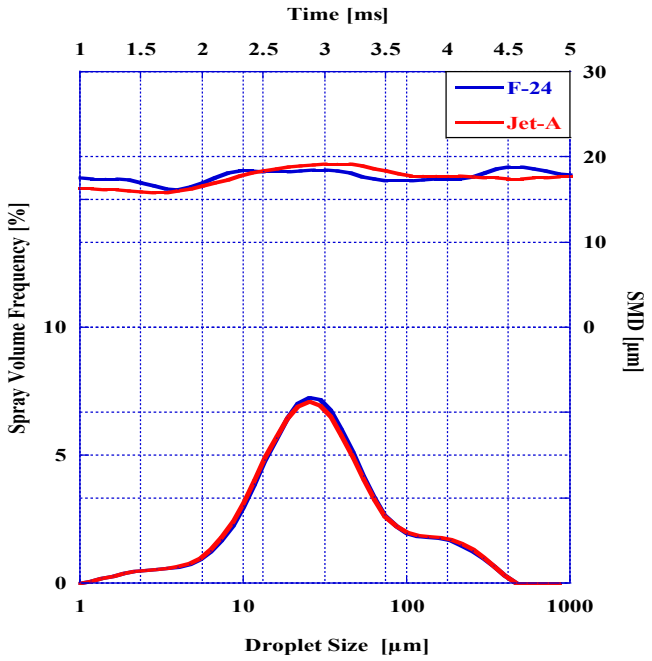

Fig. 8. Spray Development of Tested Fuels.

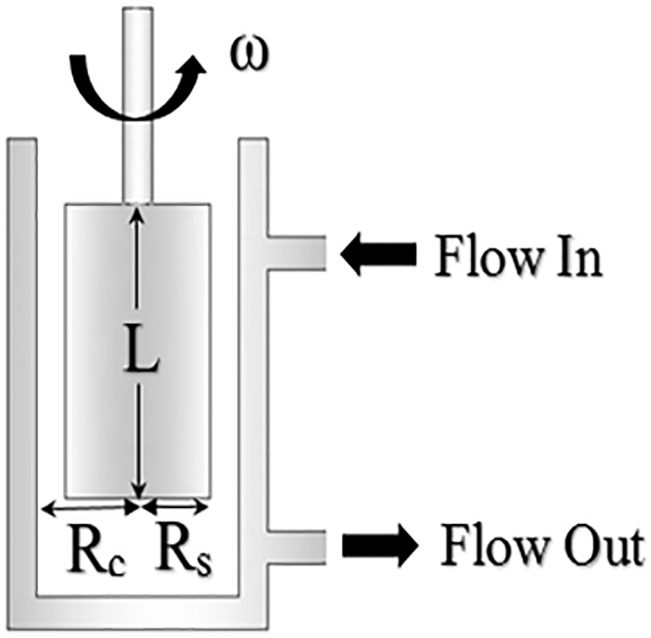

Fig. 9. Brookfield DV-II + Pro Rotational Viscometer, Spindle and Coolant Cross-Section.

Table 4
Average SMD.

	F-24	Jet-A
SMD [μm]	18.7	17.59

Table 5
Particle Size by Volume.

Particle Size by Volume	F-24	Jet-A
Dv (10) μm	9.96	9.85
Dv (50) μm	30.45	30.11
Dv (90) μm	133.33	133.45

The SC-18 spindle was submerged in approximately 7.0 mL of fuel and rotated at a speed of 200 rpm. This spindle was chosen for its compatibility with kerosene-type fuels. The fuel was then heated by a double wall jacket of coolant to determine the drop in viscosity with the increase in temperature. Viscosity was measured from 26 °C to 90 °C in increments of 2 °C. Fig. 9 displays the variables for the calculation of the shear rate and shear stress. These values were determined using Eq. (4) and Eq. (5). R_c and R_s are the radii of the container and spindle and are represented in meters; and ω is the rotational velocity of the spindle rad/sec. M represents the motor torque in Nm, and L is the length of the SC-18 spindle in contact with the fuel.

$$\dot{\gamma} = \frac{2\omega {R_c}^2}{{R_c}^2 - {R_s}^2} \tag{4}$$

$$\tau = \frac{M}{2\pi {R_s}^2 L} \tag{5}$$

Fuels' viscosity and density have a direct relationship with temperature and have a big impact on atomization, mixture formation, droplets' momentum and spray's penetration [46]. The average kinematic viscosity curve with respect to temperature for F24 and Jet-A can be seen in Fig. 10. As temperature increase because the lower viscosity and density in the test fuel. the shear stress between the wall and the spindle decreases, resulting a viscosity at 40 ℃ for F24 at 1.37 cP and 1.20 cP for Jet-A.

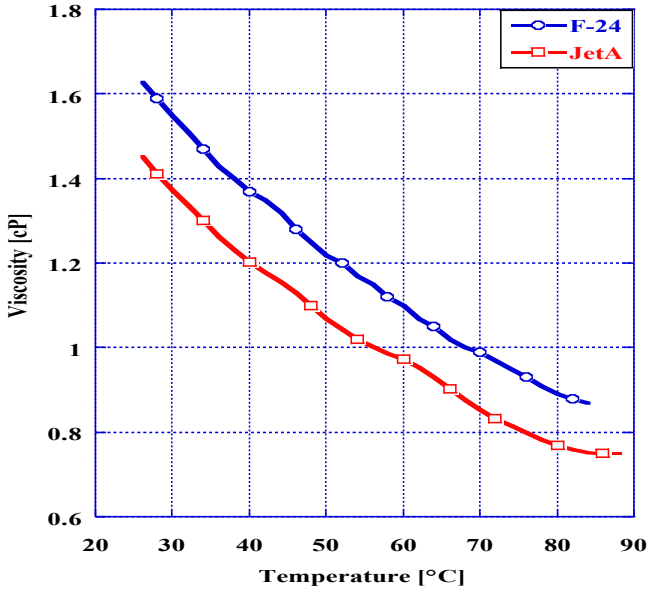

Fig. 10. Viscosity Analysis of Test Fuels.

4. CVCC methodology and DCN determination

4.1. Experimental apparatus

The PAC CID 510 is a constant volume combustion chamber (CVCC), and it was used to determine a fuel's derived cetane number (DCN) and combustion phasing. DCN is a measurement of a fuel's autoignition quality. For each combustion analysis, 5 conditioning cycles were performed in the CVCC. This was to prime the combustion chamber of the test fuel and clear any remaining fuel from previous fuels tested in the apparatus. The 5 conditioning cycles were followed by 15 full cycles of injection, combustion, and exhaust. All testing utilizes the ASTM D7668-

Table 6
ASTM D7668-14.a Testing Standard.

Combustion chamber Wall Temp.	Fuel Injection Pressure	Coolant Temp.	Injection Pulse Width	Combustion chamber Pressure
595.5 °C	1000 bar	50 °C	2.5 ms	20 bar

14.a Testing Standard in Table 6.

Fig. 11 shows the CAD models of the PAC CID 510 CVCC. The numbers on the Figure correspond to essential components in the system. Component 1 is the high-pressure common rail, component 2 is the 6-orifice BOSCH high-pressure fuel injector which provides an excellent spray pattern and atomization of the test fuel. It injects into a uniformly heated, constant volume, controlled pressure, combustion chamber labeled as component 3. Pressure changes due to combustion were measured with a piezoelectric pressure sensor shown as component 4. Additionally, injection pressure in the rail, is measured using the pressure sensor 5.

A cross sectional view of the combustion chamber is displayed in Fig. 11. In this Figure, the spray profile into the combustion chamber is shown.

4.2. Experimental procedures

The 15 combustion tests were averaged to calculate the average ID and CD for each fuel. The ID begins at start of injection, denoted as 0 ms on the timeline, and ends when LTHR is at its peak as seen in Fig. 13. The CD is the duration from start of injection to the peak of HTHR or the midpoint of the pressure curve. DCN was calculated by using the ID and CD with Eq. (6) [67,68].

$$DCN = 13.028 + \left(-\frac{5.3378}{ID}\right) + \left(\frac{300.18}{CD}\right) + \left(-\frac{12567.90}{CD^2}\right) + \left(\frac{3415.32}{CD^3}\right) \quad (6)$$

Table 7, shows the DCN and the average ID and CD for F-24 and Jet-A. The DCN for both neat fuels of Jet-A and F24 were determined to be 47.0 and 43.4. The average ID and CD of neat Jet-A was found to be 3.35 ms and 5.14 ms. The average ID of neat F24 is larger than that of neat Jet-A with a value of 4.10 ms, additionally F24 has a lower average CD at 5.79 ms. This difference in autoignition quality can be attributed to the hydrocarbon component species. Displayed in Table 1 are the percentages of component hydrocarbon compounds in Jet-A and F24. The difference in hydrocarbon percentages causes the change in the autoignition characteristics [9,12,67–72].

5. Combustion results and NVH analysis

5.1. AHRR and combustion phasing analysis

The Apparent Heat Release Rate (AHRR) is a measurement of the useable energy produced by the fuel's combustion. It is further defined in this study as the amount of energy remaining in the combustion chamber to raise the surrounding temperature during combustion. AHRR was calculated using the first law of thermodynamics as shown in Eq. (7), where appropriate compensations were made for the injection of the fuel into the closed system. The results of the calculation of AHRR derived from the pressure data can be seen in Fig. 12.

$$\frac{dQ}{dt} = \frac{1}{[\gamma - 1]} V \frac{dP}{dt} \quad (7)$$

From the AHRR curve, it is observed that while F24 and Jet-A have an LTHR of approximately equal duration, Jet-A begins combustion and reaches peak HTHR sooner than F24 as seen in Figures: 12–15. Additionally, Jet-A has a peak AHRR of 4.93 MW with F24 only reaching a peak AHRR of 4.08 MW.

The curve for AHRR has sub regions of combustion which are used to characterize the fuel's burn. These key regions are noted in this paper as the Ignition Delay (ID), Combustion Delay (CD), the Start of Combustion (SOC), the End of Combustion (EOC), Negative Temperature Coefficient (NTC) region, LTHR, and HTHR, and they are defined in this study in Fig. 13 as follows:

ID begins at start of injection, denoted in the graphs as 0 ms on the timeline, and ends when LTHR is at its peak.

The durations of the LTHR region begins once the AHRR becomes positive, continues through the NTC region and it concludes when the peak LTHR is matched by the values of HTHR.

The NTC region is the region occurring after the peak LTHR where the slope of the AHRR curve becomes negative. The conclusion of the NTC region is when the AHRR curve surpasses the peak of LTHR curve. This point defines the start of combustion and the beginning of HTHR.

CD is defined as the peak of HTHR and the midpoint of the pressure curve.

EOC is defined as the moment at which the AHRR curve crosses zero for the first time after peak HTHR.

Fluctuations in AHRR after this point are classified as ringing events.

The cool flames which occur during this two-stage ignition process were identified between 850 K and 950 K. Labels for each of these events are shown in Fig. 13 on the temperature and AHRR curves for neat F24 [30,31,73].

Notice in Fig. 13, there is a period of time when the AHRR is negative after the SOI. This is due to the fuel's vaporization that absorbs heat from inside the combustion chamber reducing the gas temperature. This temperature drop is reflected in the heat release and the pressure trace in Fig. 22 resulting in a negative value.

To highlight the two combustion regions which occur during LTHR and the region of cool flame formation, Figs. 14 and 15 show a zoom of the AHRR curve indicating these regions of combustion for Jet-A and F24. It can be seen from these graphs that the LTHR region for Jet-A and F24 are both approximately 2 ms in accordance with Table 10. The NTC region takes up a smaller portion of the total duration of LTHR for F24 when compared to Jet-A as can be seen in both Figs. 14 and 15 and in Table 10.

Table 8 displays the energy released per combustion region for F24 vs a Jet-A reference. It was found that F24 releases more of its total energy during LTHR than Jet-A at 334.3 J compared to 287.8 J for Jet-A. This accounts for 12.6% and 11.1% of the total combustion energy for F24 and Jet-A respectively as seen in Table 9. Conversely, F24 has a smaller energy release during its NTC region than Jet-A at 124.1 J compared to 133.7 J for Jet-A. This correlates to 4.68% and 5.2% of combustion energy for F24 and Jet-A.

Additionally, the durations for each combustion region were calculated and can be found in Table 10. It was found that the overall duration of LTHR was practically identical between Jet-A and F24 at approximately 2 ms. Where the difference lies, however, is in the duration of NTC region. Jet-A has a more extended NTC region at 0.72 ms while F24 has an NTC region of only 0.48 ms. This means that F24 has a longer period of cool flame formation contributing to the increase in the energy released during LTHR region when compared to Jet-A. HTHR duration and total combustion times were also found to be longer for F24 than Jet-A.

The durations of each combustion region as a percentage of total time were calculated and displayed in Table 11. Additionally, the

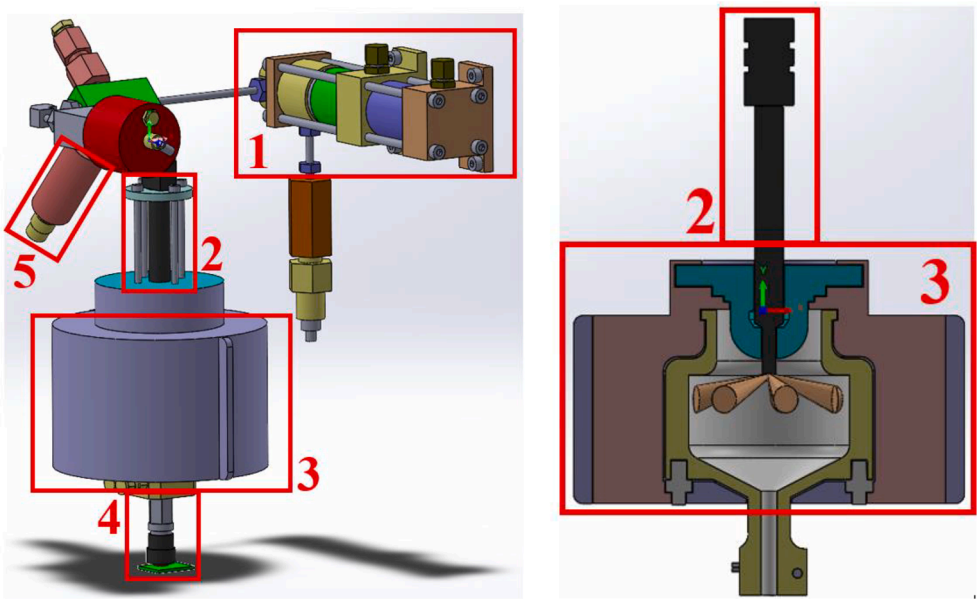

Fig. 11. PAC CID 510 Constant Volume Combustion Chamber, the components of the CVCC are listed as follows: **1.** High-Pressure Common Rail, **2.** BOSCH Injector, **3.** Combustion Chamber, **4.** Dynamic Pressure Sensor, **5.** Injection Pressure Sensor [36].

Table 7
Combustion Properties for Jet-A and F24.

Property	Jet-A	F-24
DCN	47.0	43.4
Avg. ID (ms)	3.35	4.10
Avg. CD (ms)	5.14	5.79

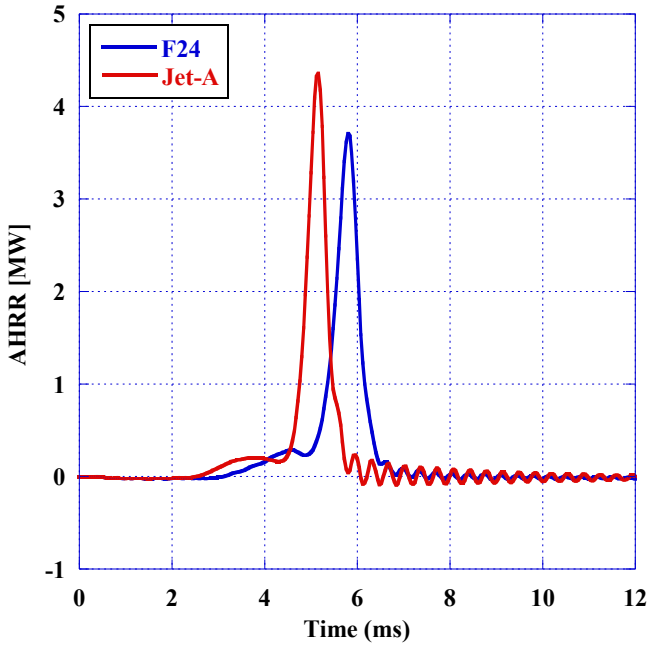

Fig. 12. AHRR for Jet-A and F24.

percent difference between Jet-A and F24 were calculated for F24 as it compares to Jet-A. It was found that, the duration of NTCR for F24 takes up a substantially smaller portion of the total combustion duration when compared to Jet-A.

These results confirm again that Jet-A and F24 have significant

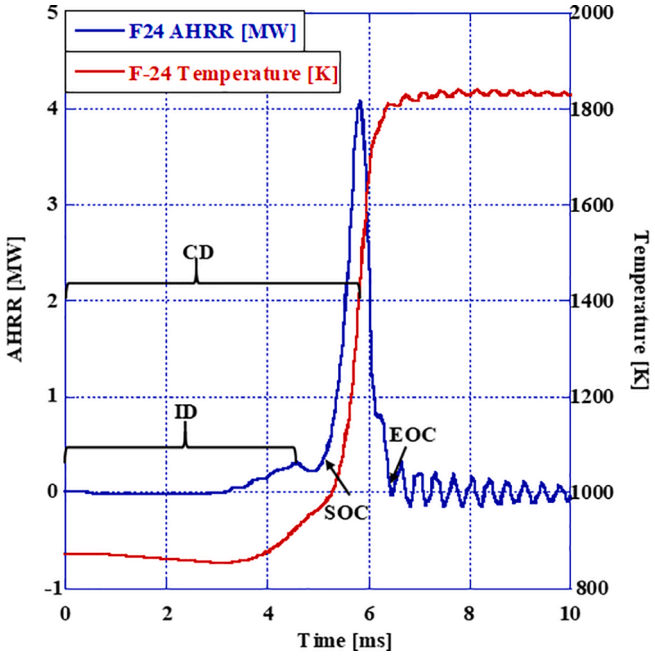

Fig. 13. Ignition Delay, Combustion Delay, Start of Combustion, and End of Combustion for F24.

Table 8
Energy Released per Combustion Region for F24 vs Jet-A Reference.

Researched Fuel	LTHR Energy Released (J)	NTC Energy Released (J)	HTHR Energy Released (J)	Total Energy
Jet-A	287.8	133.7	2302.8	2590.6
F24	334.3	124.1	2320.3	2654.1
% Change	+ 16.2%	−7.2%	+ 0.76%	+ 2.4%

difference in their combustion characteristics.

The length of these regions is important in understanding the combustion behavior and the LTHR region. The LTHR region is the period of

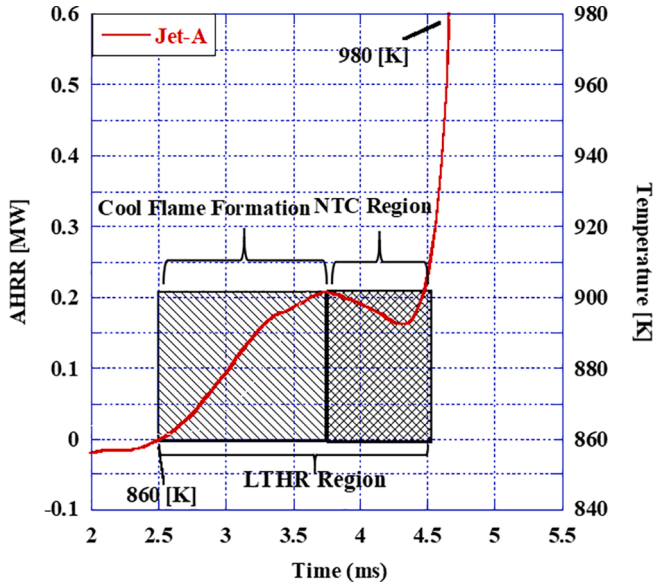

Fig. 14. Low Temperature Heat Release Region for Jet-A.

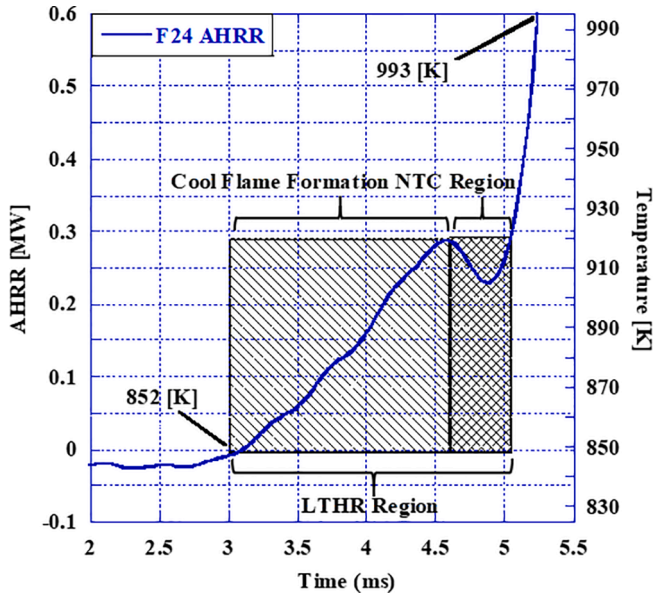

Fig. 15. Low Temperature Heat Release Region for F24.

Table 9
Energy Released per Combustion Region (%AHRR) for F24 vs Jet-A Reference.

Researched Fuel	LTHR %	NTC %	HTHR %
Jet-A	11.1	5.2	88.9
F24	12.6	4.7	87.4
% Change	+13.5	−9.6	−1.7

Table 10
Duration per Combustion Region for F24 vs Jet-A Reference.

Researched Fuel	LTHR (ms)	NTCR (ms)	HTHR (ms)	Total (ms)
Jet-A	1.96	0.72	1.56	3.52
F24	1.92	0.48	2.08	3.96
% Change	−2.0%	−38.9%	+33.4%	+12.5%

Table 11
(%AHRR), Total Combustion Duration Percentages for F24 vs Jet-A Reference.

Researched Fuel	LTHR %	NTCR %	HTHR %
Jet-A	55.7	20.5	44.3
F24	48	12	52
% Change	−13.8%	−41.4%	+17.4%

combustion where heavy peroxides and radicals are rapidly formed and temperatures are too low to initiate autoignition [31,32,74–76]. Fuels which have a larger quantity of complex hydrocarbons will experience an extended period of LTHR [31,32]. These complex hydrocarbons break down into radicals, peroxides, and aldehydes, and cool flames are formed, decay, and quench in rapid succession [31,32]. After the region of cool flame formation, there is a period of increased peroxide formation of predominantly ketohydroperoxides. This compound has a large energy of formation and is predominant in during the NTCR. This region is characterized by this compound as it takes more energy to form than is released from its combustion [74].

F24 was found to have an extended region of cool flame formation when compared to Jet-A. Given that the duration for LTHR is practically identical between F24 and Jet-A, the combustion of F24 has a reduced NTC region as well. The greater relative period of cool flame formation during the combustion of F24 contributes to an increase in combustion stability and a reduction in ringing. A zoom of the LTHR for F24 and Jet-A is displayed in Fig. 16.

5.1.1. *Combustion temperature analysis*

Combustion temperature was derived from the measured pressure data and the known volume of the combustion chamber. The temperature traces for Jet-A and F24 are presented in Fig. 17. The temperatures and time for each combustion region are shown in Table 12. The combustion of F24 reached a higher temperature after LTHR temperature when compared to Jet-A.

In alignment with the determinations for the combustion regions in relation to the AHRR, the combustion regions in terms of temperature have been outlined in Figs. 18 and 19. While there is a delay of half a millisecond between the beginning of LTHR for F24 when compared to Jet-A, F24 begins LTHR at a lower temperature and ends at a higher temperature than that of Jet-A. There can also be seen a faster increase in the temperature during LTHR for F24 than that of Jet-A. This increase

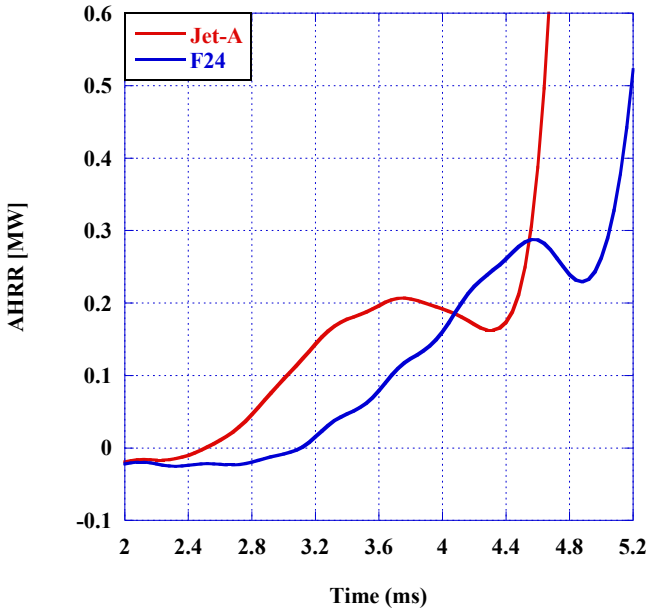

Fig. 16. Low Temperature Heat Release (LTHR) Region for F24 and Jet-A.

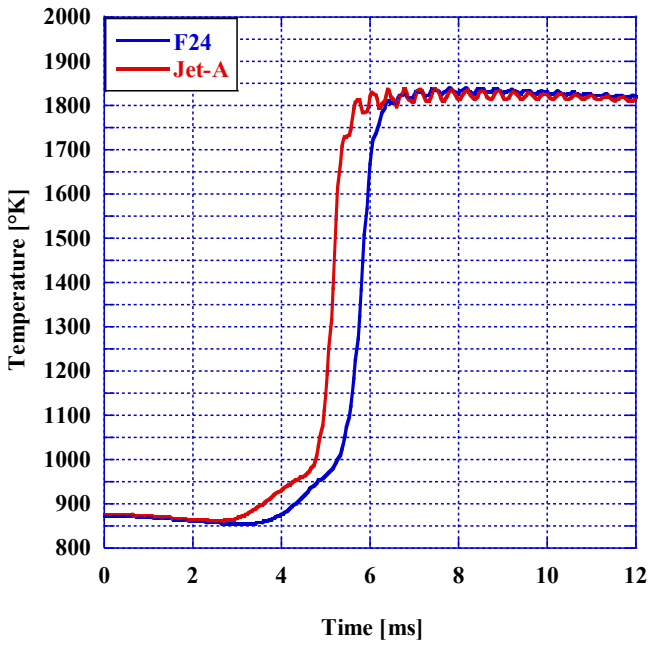

Fig. 17. Combustion Temperature for Jet-A and F24.

Table 12
Combustion Temperatures at each phase.

Researched Fuel	LTHR Temp [K] (Start/ End)	LTHR Peak [K] (Temp/ Time)	NTC Temp [K] (Start/ End)	NTC Valley [K] (Temp/ Time)
Jet-A	861.2/961.3	913.4/ 3.76 ms	913.4/961.3	952.1/ 4.32 ms
F24	852.0/967.8	923.3/ 4.56 ms	923.3/967.8	951.8/ 4.84 ms

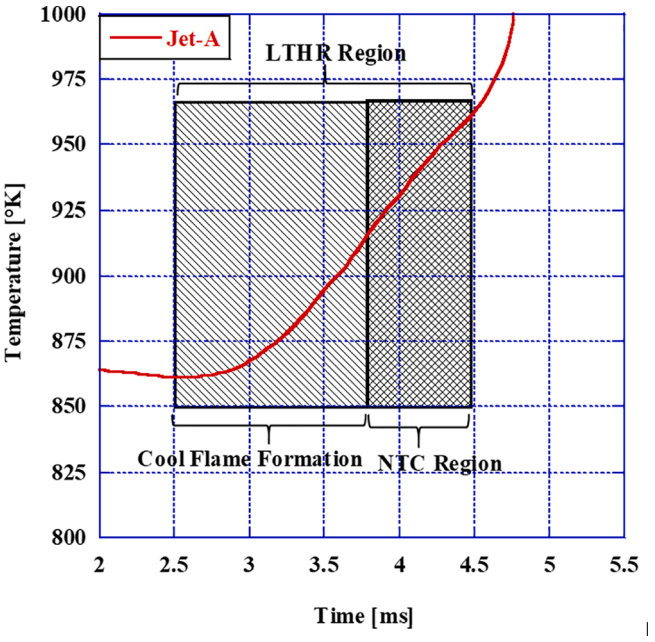

Fig. 18. Combustion Regions by Temperature for Jet-A.

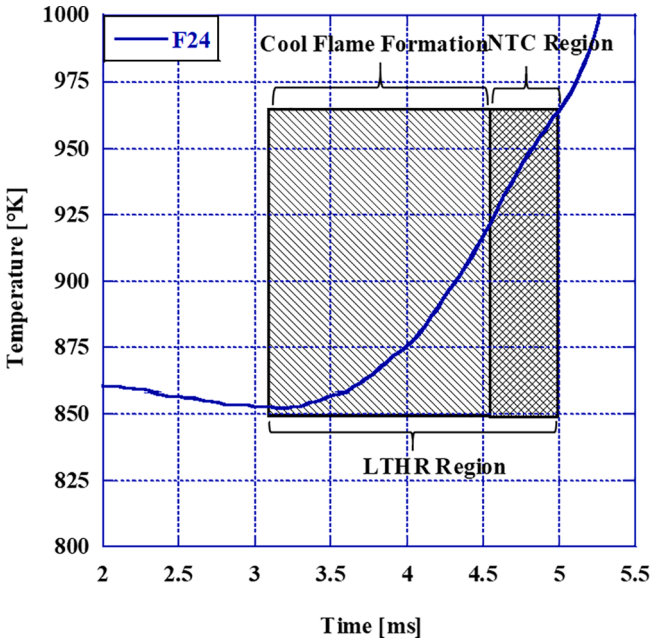

Fig. 19. Combustion Regions by Temperature for F24.

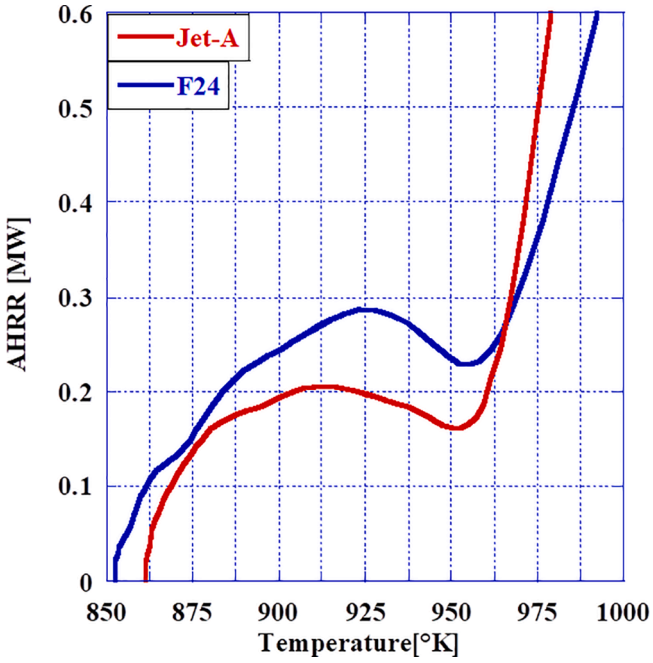

Fig. 20. AHRR vs Temperature for F24 and Jet-A.

in the region of cool flame formation increases the total energy released by the fuel during combustion without a significant decrease in the performance of the engine.

In Fig. 20, the AHRR and temperature of the LTHR regions of Jet-A and F-24 are analyzed starting from the point at which AHRR becomes positive. This illustrates the fuel's energy release within an environment of increasing temperature. During this temperature increase, both fuels undergo a period of cool flame formation and quench. This is the same region highlighted in Figs. 14, 15, 18, and 19. This is observed from approx. 850 °C to 935 °C as the fluctuations of slope as they reach their peak AHRR value during their respective LTHR phase.

After the cool flame formation peaks, NTC region begins. This region develops due to the rapid formation of branch-chaining intermediates

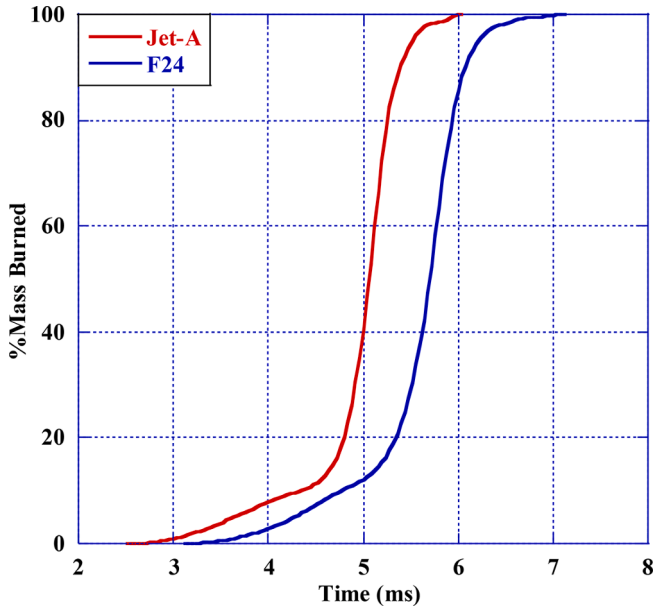

Fig. 21. Percent Mass Burned for Jet-A and F24.

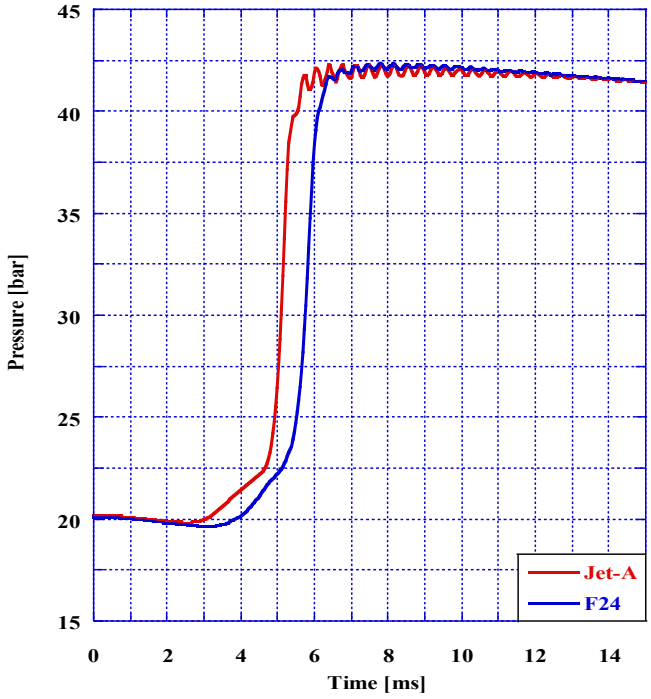

Fig. 22. Combustion Pressure Trace for Jet-A and F24.

while temperature increases. This rapid formation of aldehydes causes the fuel to undergo a period of negative energy release even though temperatures in the chamber are increasing. The existence of the NTC is fundamentally responsible for the formation of stable cool flames [33]. This is also defined as the temperature for which ketohydroproxides formations is at its maximum [33].

As displayed in Table 12, there is a threshold in the energy release for which Jet-A and F24 burn started increasing the temperature in the combustion chamber. Those temperature have been identified as 861.2 K and 852 K for F24 and Jet-A, respectively. F24 was found to have a higher peak LTHR temperature at 925 K when compared to Jet-A at 912.5 K, however the HTHR has a reduced slope compared to Jet- A, as observed in Fig. 22, resulting in the same peak temperature between the two fuels. The oxidation process of F24 creates higher temperatures during LTHR and propagates over a longer period during entire combustion compared to Jet-A. F24′s oxidation process occurs over higher temperatures in the LTHR, and reduced pressure rise rate during HTHR creates a scenario for which F24 burns with greater stability and this will be further discussed in the ringing analysis. Jet -A has the inverse correlation where energy release increases more rapidly during HTHR with lower LTHR temperature compared to F24.

5.1.2. Mass Fraction burned (MFB)

The shorter ignition and combustion delay for Jet-A results in a higher DCN, which correlates to a better auto-ignition quality. This quicker combustion rate can also be seen in the percent mass of the fuel burned and this calculation is shown in Fig. 21.

The determination of these values indicates that Jet-A combusts quicker than F24 having burned all of its injected mass by 6.04 ms compared to F24 which completes its combustion over a millisecond later at 7.12 ms after start of injection. These results confirm again that Jet-A and F24 have a significant difference in their combustion characteristics.

5.2. Combustion pressure and ringing analysis

Pressure data in the combustion chamber was obtained through the piezoelectric pressure sensor over the course of 15 cycles. The pressure data from each of the cycles was collected, then averaged and can be seen in Fig. 22. This averaged data was used to calculate AHRR.

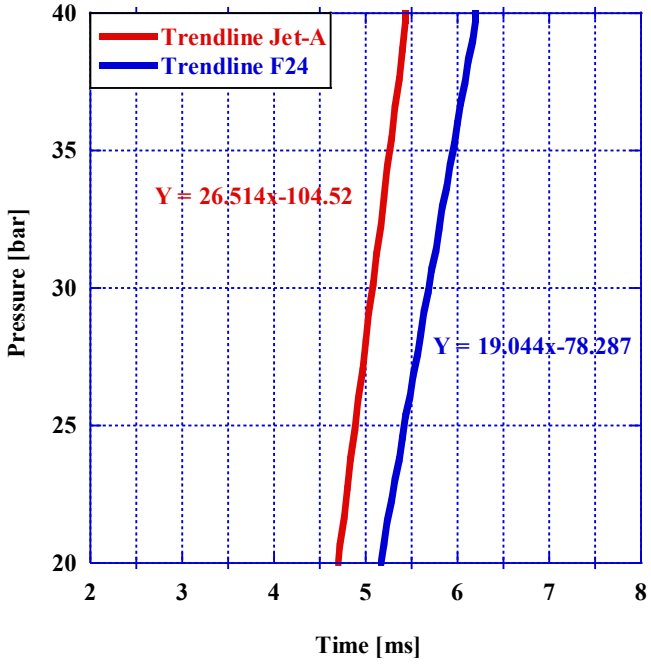

Fig. 23. Pressure Trendlines during Combustion for Jet-A and F24.

Fig. 23 represents the trendlines for the pressure trace of Jet-A and F24. A linear representation was determined from the pressure values between the start and end of combustion. This was done to illustrate and

Table 13
Peak Pressure of Researched Fuel.

Researched Fuel	Peak Pressure (bar)
Jet-A	42.32
F24	42.34

further understand the burn rate of each fuel. From this determination, it was found that F24 has a slower burn rate and flame front propagation than Jet-A as represented by a shallower slope in the trendline. In addition to the delay in combustion, F24 has a slower flame propagation and a more gradual increase in pressure.

The peak pressures for Jet-A and F24 are shown in Table 1. After SOI, the pressure trace crosses below 20 bar, and then proceeds with a sharp positive slope upwards. The initial reduction in pressure from the set-point of 20 bar is due to the injected fuel's heat absorption during vaporization that is causing a drop in temperature in the combustion chamber. The maximum average pressure for F-24 was found to be 42.34 bar, while Jet-A was found to be 42.32 bar as seen in Table 13. The percent difference between the peak pressure of Jet-A and the peak pressure of F24 was 0.047%. This small difference is within the tolerance of the dynamic pressure sensor in the CVCC. However, despite having similar peak pressures, it was found that the larger the increase in the combustion chamber pressure rise rate (PRR) resulted in greater combustion instabilities. This was indicated by the greater magnitude of the resulting ringing.

Fig. 24 is a zoom of the peak pressure, where the only the pressure between 5 and 25 ms and 40 and 43 bar is shown, for Jet-A and F24 to show the ringing. Figs. 25, 26, and 27 are the determinations for the ringing due to combustion based on the oscillations in the pressure trace. For the two curves in each Figure, the maximums and minimums for the pressure oscillations were taken and are represented by a smooth curve. Magnitude of each oscillation was then determined by taking the difference between the maximum and minimum values. The magnitude values for Jet-A and F24 were then displayed as a continuous curve in Fig. 23. It was found that although F24 had a very similar peak pressure to Jet-A, the magnitude of the oscillations for F24 were much smaller than that of Jet-A reaching a peak magnitude of 0.28 bar compared to 0.9 bar for Jet-A. This indicates that F24 has a higher combustion stability than that of Jet-A. Additionally, the peak oscillation amplitude for F24 occurs almost 2 ms later than that of Jet-A due to the longer period of LTHR for F24.

Both fuels experienced an exponential reduction in the ringing amplitude after reaching peak pressure. A trendline was determined in order to quantify the difference in pressure oscillations between Jet-A and F24, using Eq. (8). Where b and k represent changes in the slope of the trendline for the two curves in Fig. 27.

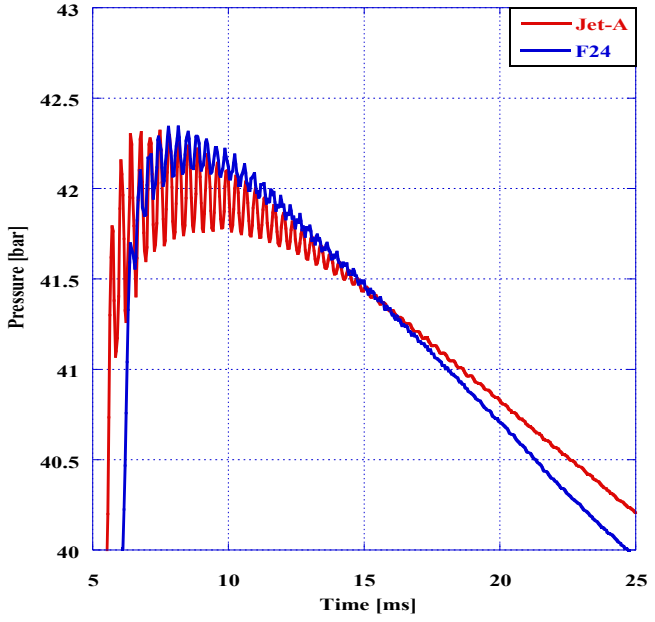

Fig. 24. Ringing at Peak Pressure for Jet-A and F24.

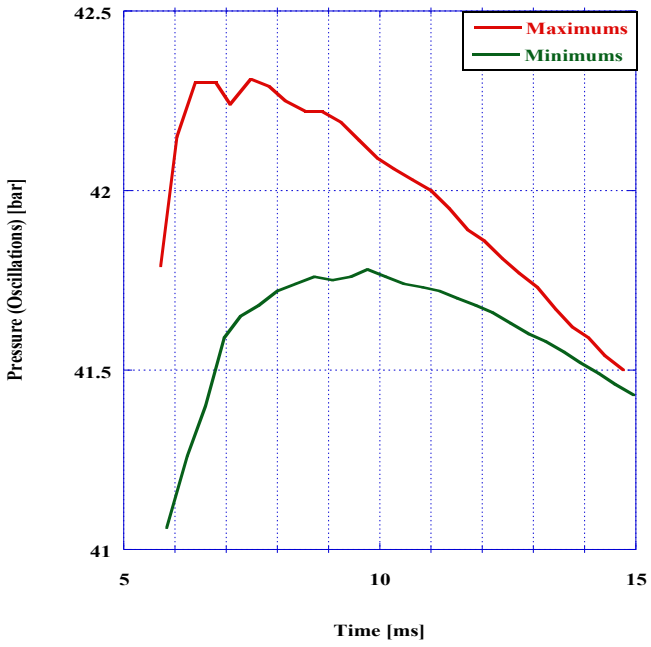

Fig. 25. Ringing Limits/Magnitude in the Pressure Trace for Jet-A.

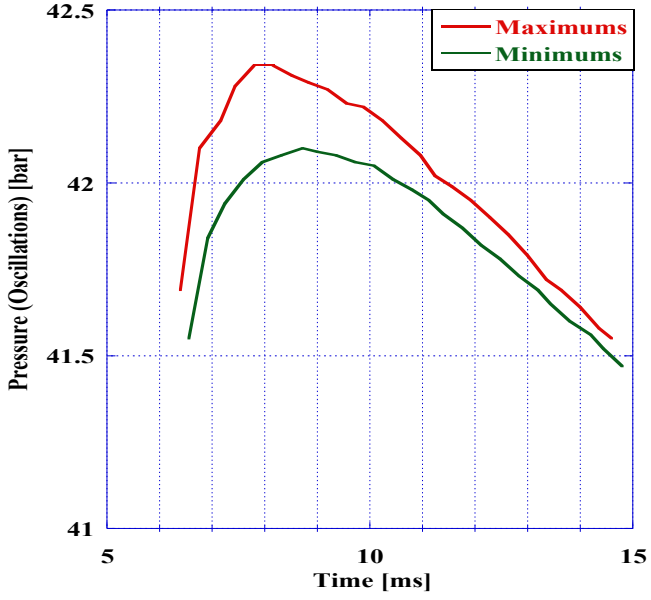

Fig. 26. Ringing Limits/Magnitude in the Pressure Trace for F24.

$$y = be^{kx} \tag{8}$$

Between F24 and Jet-A, there is a much steeper slope associated with the oscillation convergence of Jet-A over F24. This is apparent as the b value for Jet-A is 4.8 compared to 0.78 for F24. Additionally, the k value for F24 was significantly smaller with a value of −0.158 compared to the k value for Jet-A at −0.267. While Both fuels converge at approximately the same ringing amplitude at 15 ms, Jet-A produces a much greater ringing intensity with a more aggressive decrease than F24. This is an indication that F24 has a more stable combustion than that of Jet-A. The equations of the trendline for Jet-A and F24 can be seen in Eq. (9) and Eq. (10) respectively.

$$y = 4.8038e^{-0.267x} \tag{9}$$

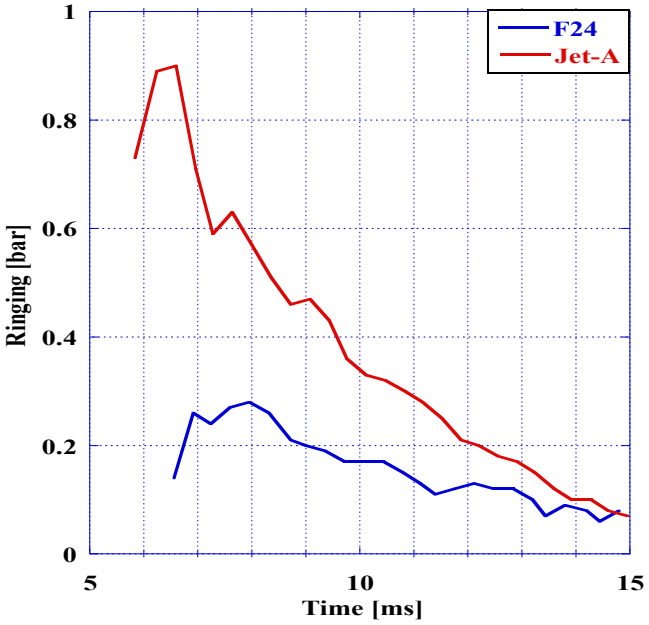

Fig. 27. Magnitude of Ringing for Jet-A and F24.

$$y = 0.7832e^{-0.158x} \quad (10)$$

The reduction in the pressure oscillations after combustion indicates that the combustion of F24 is more stable than that of Jet-A. This correlated to the extended region of cool flame formation outlined in section 5.2. Cool flames were found having a significant impact on the ignition timing, burn rate, burn limit, and engine knock [9]. The extended region of cool flame region is attributed in this paper to the high percentage of olefins and cyclohexanes, present in F24 as seen in Table 1. Olefins give also low luminosity cool flames with longer induction periods compared to other hydrocarbons [31] and confirmed in Figs. 14 and 15.

5.3. Noise, vibrations and Harshness analysis

An NVH investigation was conducted on the combustion events of F-24 and Jet-A in a PAC CID 510 CVCC instrumented with a Brüel and Kjær charge accelerometer (Type 4326 A- 001) to measure the vibrations produced during the combustion cycle. The data acquisition system utilized to collect the combustion induced vibrations included a Brüel & Kjær Type 3050-A-060 data acquisition board in which frequencies from 0 Hz to 25.6 kHz were evaluated. Post processing was conducted with the Brüel & Kjær application BK Connect (2020 edition) and the accelerations (m/s^2) produced from the combustion of Jet A and F24 were evaluated in relation to combustion phenomena and timing as discussed previously for each fuel. The combustion event in relation to the AHRR has a duration of ten milliseconds and it is within this time that the combustion vibrations for each fuel were evaluated.

To collect the vibrations produced during the combustion sequence of the CVCC, an accelerometer was placed upon the top face of the combustion chamber which can be seen in Figs. 28 and 29. The axes of the accelerometer include the X-Y plane spanning across the radial face of the CVCC and the Z axis being parallel to the vertical axis of the CVCC and the injector, as depicted in Figs. 28 and 29. The Brüel & Kjaer Type 4326 A-001 accelerometer was used in the experimental evaluation of the vibrations measured in the Z-direction included representation of the combustion shockwave propagation across the CVCC for both Jet-A and F24.

Throughout the DCN determination it was evaluated that the ID of F24 was approximately 1 ms in duration longer than that of Jet-A. This relationship was confirmed in the combustion produced vibrations, as seen in Figs. 31 and 32, where the vibrations during the ignition delay for F24 were almost one millisecond longer than the ignition delay vibrations for Jet A. From the combustion vibrations recorded for Jet A and F24, it was found a good correlation with the peak value of AHRR for Jet A (4.93 MW) produced a greater magnitude vibration than the peak AHRR of F24 (4.08 MW). The greatest magnitude of acceleration collected for Jet A was 29.65 m/s^2 and occurred at the ignition timing of the combustion event. Regarding the greatest magnitude of acceleration collected for F24, a 19.96 m/s^2 magnitude of acceleration was observed also at the ignition timing of the combustion event. This correlation shows that as the peak AHRR increases, greater magnitudes of vibrations can be expected as was evident when comparing Jet-A and F24.

For both Jet A and F24, combustion ringing vibrations were recorded immediately after the HTHR region. These diminish in magnitude as the combustion pressure wave reflects successively in the combustion chamber. This can be correlated to the combustion pressure wave propagating from the ignition site to the chamber's wall and then reflects back, towards ignition site, or top of the combustion chamber again. With each consecutive reflection of the combustion pressure wave within the combustion chamber, ringing was produced. This ringing was observed in the pressure trace in Figs. 22 and 24. As the pressure signal of the CVCC diminishes in magnitude with each consecutive wave

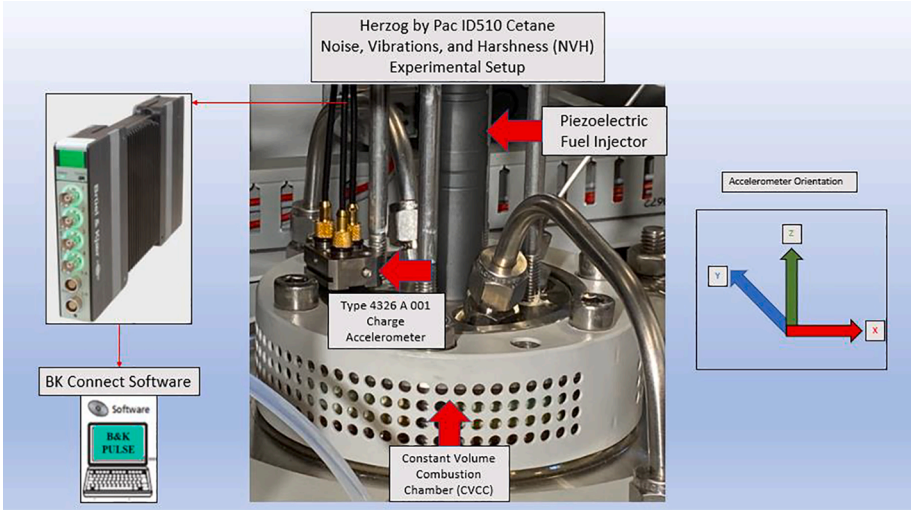

Fig. 28. NVH Instrumentation on the Constant Volume Combustion Chamber.

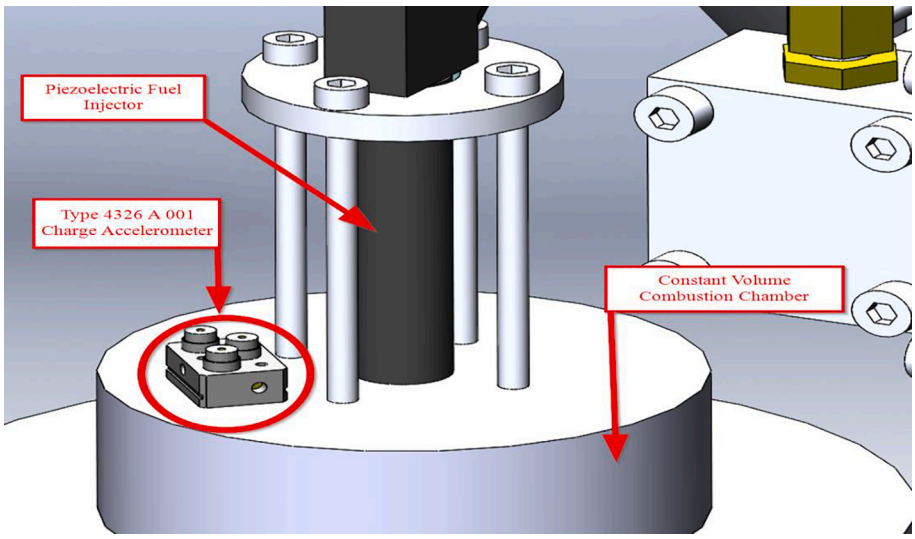

Fig. 29. Accelerometer Instrumentation on the CVCC (Solid Modelling).

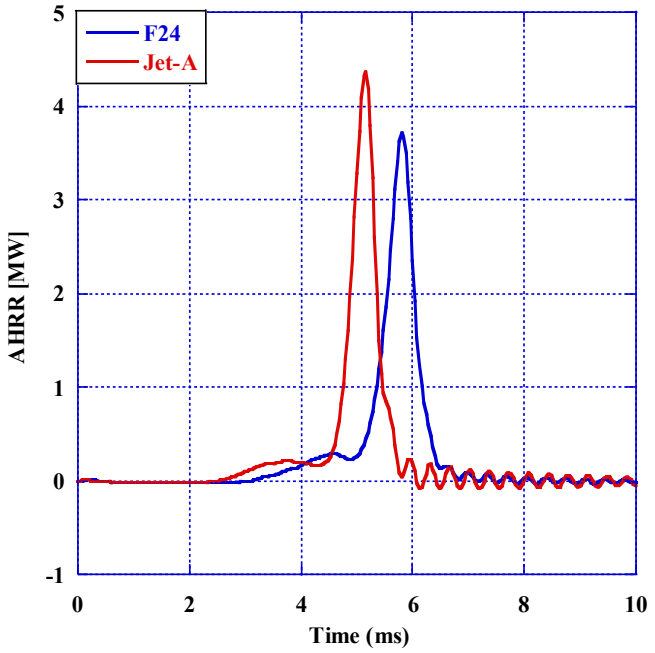

Fig. 30. AHRR for Jet-A and F24.

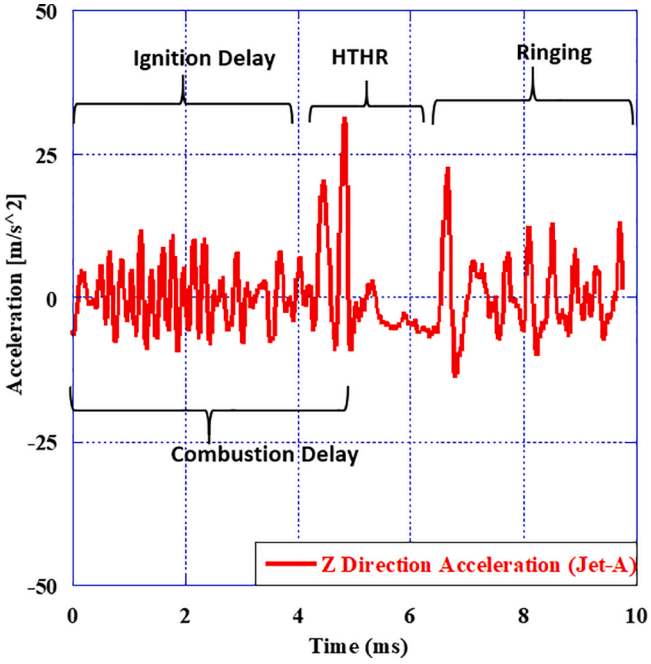

Fig. 31. Z Direction Acceleration Signatures with relation to the HTHR of Jet A.

period of the combustion sequence, a diminishing vibrations' magnitude can be evaluated as the combustion wave rings across the CVCC. Throughout the ten millisecond combustion vibrations recording of the CVCC, the greatest magnitude of vibrations occurs at the beginning of HTHR for both Jet A and F24 and diminishes in magnitude naturally as the combustion wave propagates throughout the CVCC.

From the NVH results in the Z direction it was observed that after the ignition event, the vibrations from the combustion event have a rather flatline region during the HTHR for both fuels and this paper would report this phenomenon for the first time in the literature. The accelerometer was positioned opposite to the dynamic pressure sensor where the location of the pressure sensor enables the sensor to detect the rapid pressure increase caused by combustion. The flatline seen in the acceleration waveforms of Jet A and F24 can be explained as the time required for the pressure wave to reflect off the bottom of the combustion chamber and return to the top of the chamber as seen in Figs. 31-32. The combustion induced vibrations detected by the accelerometer are the reflections of the main combustion event off the bottom of the combustion chamber. A graph of the AHRR has been included in Fig. 30 for reference when discussing the regions of combustion for Jet-A and F24.

The approximate Z-direction height of the CVCC is 0.097 m and the air–fuel mixture was assumed to be an ideal gas. From evaluating the CVCC combustion chamber pressure at the end of Combustion Delay, the in-cylinder temperature was derived to be approximately 1400° Kelvin. At this temperature, it was calculated that the speed of sound within the CVCC was approximately 750 m/s and it was then calculated that the maximum amount of time for the pressure wave to propagate to the bottom of the cylinder was 0.13 ms. The combustion pressure wave propagation time of 0.13 ms across the CVCC equates to approximately 3.5 reflections of the combustion pressure wave per ms. As is supported by Figs. 31 and 32, approximately 3.5 peaks and troughs which correlate to the reflection of the combustion pressure wave between the top and bottom faces of the CVCC can be counted per millisecond.

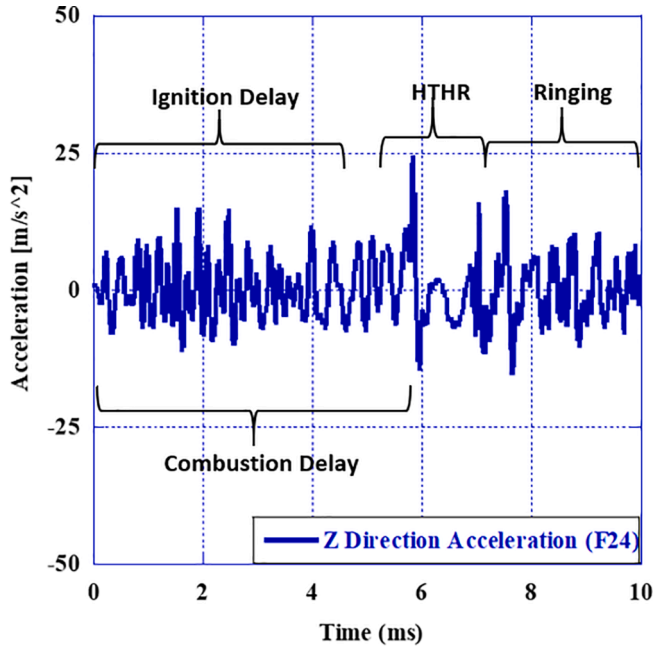

Fig. 32. Z Direction Combustion Acceleration Signatures with relation to the Apparent Heat Release Rate (AHRR) of F24.

The NVH investigations determined that there is a strong connection between the two primary combustion phases, ID and CD, and the vibrations produced. Furthermore, the lower magnitude of pressure shockwaves produced from F24′s combustion correlate to a decrease in the magnitude of the measured vibrations by approximately 0.5 g for F24 when compared to Jet-A. During the HTHR, the lowest vibrations have been recorded during the combustion cycle for both fuels.

6. Conclusion

For this study, two aviation fuels, 100% F24 and 100% Jet-A were investigated in a constant volume combustion chamber to determine their combustion and NVH characteristics. This study includes a unique comprehensive fuel analysis on F24 and Jet-A using consistent POSF numbers for all the investigations into the thermophysical and combustion properties.

F24 was found to have has a significantly higher concentration of olefins and cyclohexanes when compared to Jet-A. The details of the Low Temperature Heat Release (LTHR) properties of each fuel as well as the vibrations produced from combustion instabilities were investigated. The LTHR region is described in this paper, by two distinct regions: the region of cool flame formation and the Negative Temperature Coefficient Region (NTCR). These regions were analyzed for their durations as well as the amount of energy released for each burn period. A multitude of fuel tests were also conducted to determine the thermophysical properties of each fuel and their influence on combustion.

A calorimetry analysis was conducted to determine the lower heating value of each fuel. It was found that the average lower heating value for both fuels are approx. 41.85 MJ/kg, ±0.1%. This was determined to be within the sensitivity of the instrument and relates back to the nearly identical H/C ratio of the two fuels as seen in Table 1.

A differential thermal analysis and a thermogravimetric analysis were conducted to determine the absorption and release of energy and vaporization rate of each researched fuel at lower temperatures. It was found that Jet-A has a higher volatility than that of F24 and starts a vaporizing process at a lower temperature compared to F24. This is more favorable for combustion as fuels with a higher volatility form a homogeneous air–fuel mixture more rapidly and at a lower temperature. There was observed a second endothermic and exothermic reaction in the DTA for Jet-A between 300 °C and 500 °C. On the other hand, F24 was observed to have two additional areas of endothermic and exothermic reactions at 250 °C to 350 °C and 425 °C to 550 °C both with a lower magnitude.

A viscosity and spray analysis were conducted using a Brookfield DV-II + Pro rotational viscometer and a Mie scattering He-Ne laser respectively. F24 was found to have a higher viscosity at 40 ℃ at 1.37 cP compared to 1.20 cP for Jet-A. The Mie scattering laser was used to determine the spray profile, droplet distribution and mixture formation for each of the researched fuels. The viscosity values were found to correlate to a larger SMD for F24 at 18.7 μm compared to 17.59 μm for Jet-A. A smaller SMD is associated with a better mixing and complete combustion as the droplets have a larger surface area to volume ratio.

The Ignition Delay (ID) and Combustion Delay (CD) were researched to find the DCN of each fuel utilizing a PAC CID 510 constant volume combustion chamber (CVCC) at the ASTM D7668-14.a standard and were determined from an average of 15 combustion cycles for each of the researched fuels. The ignition delay and combustion delay for F-24 was found to be 4.04 ms and 5.71 ms with a DCN resulting at 43.77. Jet-A was found to have a higher DCN of 47 with an ignition delay and combustion delay of 3.35 ms and 5.14 ms. It was also found that Jet-A has more favorable autoignition characteristics than F24. Peak pressure during the fuels' combustion was found to be almost identical with a percent difference of only 0.047%.

For the LTHR analysis, it was found that the fuels have a nearly identical duration for LTHR at approximately 2 ms. F24, however, has a much shorter NTCR than that of Jet-A. This means that during LTHR, F24 has an extended region of cool flame formation and therefore releases more of its energy during LTHR than Jet-A at 334.3 J and 287.8 J respectively. Additionally, F24 reaches a lower peak AHRR than Jet-A at 4.08 MW compared to 4.93 MW for Jet-A accounting for 12.6% and 11% of total energy released during combustion for each fuel. Given the identicality in the duration of LTHR between Jet-A and F24, the extended region of cool flame formation in F24 contributes to an increase in combustion stability and a reduction in ringing.

Analysis of the pressure trace revealed that F24 has a lower pressure rise rate after LTHR than Jet-A. This indicates that F24 has a slower burn rate and flame front propagation. A ringing investigation was conducted on the measured pressure oscillations in the combustion chamber at peak pressure for Jet-A and F24. It was found that the magnitude of the ringing for Jet-A was 3x higher than that of F24 reaching a magnitude of 0.9 bar and 0.28 bar respectively. Additionally, it was found that with an exponential trendline, F24 had a much flatter curve with a smaller y-intercept than that of Jet-A. This suggests that F24 has a higher combustion stability than Jet-A.

The NVH investigations determined that there is a strong connection between the two primary combustion phases, ID and CD, and the vibrations produced from combustion. The ID and CD regions during the combustion were found to produce longer duration of vibrations for F24. This correlated to the longer durations for these combustion phases for F24 when compared to Jet-A. Furthermore, the lower magnitude of pressure shockwaves produced from F24′s combustion correlate to a decrease in the magnitude of the measured vibrations by approximately 0.5 g for F24 when compared to Jet-A. During the HTHR, the lowest vibrations have been recorded during the combustion cycle for both fuels.

CRediT authorship contribution statement

Valentin Soloiu: Conceptualization, Methodology, Validation, Investigation, Resources, Supervision, Project administration, Funding acquisition. **Amanda Weaver:** Conceptualization, Methodology, Validation, Formal analysis, Investigation, Writing – original draft, Writing – review & editing. **Lily Parker:** Formal analysis, Investigation, Writing – original draft. **Austin Brant:** Formal analysis, Investigation, Writing – original draft, Writing – review & editing. **Richard Smith:** Formal

analysis, Investigation, Writing – original draft, Writing – review & editing. **Marcel Ilie:** Investigation, Formal analysis. **Gustavo Molina:** Investigation, Formal analysis. **Cesar Carapia:** Formal analysis, Investigation, Writing – original draft.

Declaration of Competing Interest

The authors declare the following financial interests/personal relationships which may be considered as potential competing interests: Valentin Soloiu reports financial support was provided by National Science Foundation. Valentin Soloiu reports a relationship with National Science Foundation that includes: funding grants.

Acknowledgments

We acknowledge the contribution of the Air Force Laboratory for suppling the experimental fuels, Christopher Mileski, Charles McGuffy, Michael Rankin, Denise Mukes, Jacques Lapeyre, from PACLP, and Joseph von Wolfgang from Malvern Lasers. Coty Harrison from Yokogawa, Tanner Smith, Tony Frazer, Ryan Salmon, and Alfonso Moreira from Brüel and Kjær. Finally, we would like to acknowledge R. Smith Jr. for this supporting this endeavor. This paper is based upon work supported by the National Science Foundation Grant No. 1950207.

References

[1] Riboldi CED. An optimal approach to the preliminary design of small hybrid-electric aircraft. Aerospace Science and Technology 2018;81:14–31.
[2] D. C. Bell, J. S. Heyne, S. H. Won, and F. L. Dryer, "The impact of preferential vaporization on lean blowout in a referee combustor at figure of merit conditions," Volume 1: Fuels, Combustion, and Material Handling; Combustion Turbines Combined Cycles; Boilers and Heat Recovery Steam Generators; Virtual Plant and Cyber-Physical Systems; Plant Development and Construction; Renewable Energy Systems, 2018.
[3] Goyal H, Kook S. Ignition process of gasoline compression ignition (GCI) combustion in a small-bore optical engine. Fuel 2019;256:115844.
[4] Hanyu Chen, Xi Wang, Zhixiang Pan, "Effect of operating conditions on the chemical composition, morphology, and nano-structure of particulate emissions in a light hydrocarbon premixed charge compression ignition (PCCI) engine", *Science of The Total Environment*, Volume 750, 2021, 141716, ISSN 0048-9697, https://doi.org/10.1016/j.scitotenv.2020.141716.
[5] V. Soloiu, R. Gaubert, M. Muinos, J. Moncada, T. Beyerl, G. Molina, and J. Williams, "Performance of an indirect injected engine operated with ULSD#2 blended with Fischer-Tropsch synthetic kerosene," *SAE 2017-01-1283 Technical Paper Series*, 2017, https://doi.org/10.4271/2017-01-1283.
[6] K. Ju, "Numerical study on premixed charge compression ignition (PCCI) combustion for down-sized diesel engine using converge," *SAE 2020-32-2308 Technical Paper Series*, 2020, DOI: https://doi.org/10.4271/2020-32-2308.
[7] Li Y, Jia M, Chang Y, Xie M, Reitz RD. Towards a comprehensive understanding of the influence of fuel properties on the combustion characteristics of a RCCI (reactivity controlled compression ignition) engine. Energy 2016;99:69–82.
[8] Muhammad Umer Waqas, Alexander Hoth, Christopher P. Kolodziej, Toby Rockstroh, Jorge Pulpeiro Gonzalez, Bengt Johansson, "Detection of low Temperature heat release (LTHR) in the standard Cooperative Fuel Research (CFR) engine in both SI and HCCI combustion modes", *Fuel*, Volume 256, 2019, 115745, ISSN 0016-2361, https://doi.org/10.1016/j.fuel.2019.115745.
[9] Guzman J, Brezinsky K. Experimental and modeling study of the oxidation of F-24 jet fuel, and its mixture with an iso-paraffinic synthetic jet fuel, ATJ. Combustion and Flame 2021;224:108–25.
[10] Elvers B, Andrea S. Handbook of Fuels: Energy Sources for transportation. Weinheim, Germany: Wiley-VCH; 2022.
[11] Wang X, Jia T, Pan L, Liu Q, Fang Y, Zou J-J, et al. Review on the Relationship Between Liquid Aerospace Fuel Composition and Their Physicochemical Properties. Transactions of Tianjin University 2020;27(2):87–109.
[12] Govindaraju PB, Ihme M. Formulation of optimal surrogate descriptions of fuels considering sensitivities to experimental uncertainties. Combustion and Flame 2018;188:337–56.
[13] Elmalik EE, Raza B, Warrag S, Ramadhan H, Alborzi E, Elbashir NO. Role of hydrocarbon building blocks on gas-to-liquid derived synthetic jet fuel characteristics. Industrial & Engineering Chemistry Research 2013;53(5):1856–65.
[14] Han X, Liszka M, Xu R, Brezinsky K, Wang H. A high pressure shock tube study of pyrolysis of real jet fuel jet a. Proceedings of the Combustion Institute 2019;37(1):189–96.
[15] Xu R, Chen D, Wang K, Wang H. A comparative study of combustion chemistry of conventional and alternative jet fuels with hybrid chemistry approach. 55th AIAA Aerospace Sciences Meeting. 2017.
[16] K. Kim, K. Min, J. Temme, C.-B. Kweon, and T. Lee, "Effects of F-24/ATJ blend composition on ignition kinetics at low temperatures," *AIAA Scitech 2020 Forum*, 2020.
[17] J. T. Edwards, "JET FUEL PROPERTIES," *https://www.afrl.af.mil/*. [Online]. Available: https://apps.dtic.mil/sti/pdfs/AD1093317.pdf. Jan, 2020.
[18] Kang D, Kim D, Kalaskar V, Violi A, Boehman A. Experimental characterization of jet fuels under engine relevant conditions – Part 1: Effect of chemical composition on autoignition of conventional and alternative jet fuels. Fuel 2019;239:1388–404.
[19] Ryu JI, Kim K, Min K, Scarcelli R, Som S, Kim KS, et al. Data-driven chemical kinetic reaction mechanism for F-24 jet fuel ignition. Fuel 2021;290:119508.
[20] Kumar K, Sung C-J. An experimental study of the autoignition characteristics of conventional jet fuel/oxidizer mixtures: Jet-A and JP-8. Combustion and Flame 2010;157(4):676–85.
[21] Manigandan S, Atabani AE, Ponnusamy VK, Gunasekar P. Impact of additives in jet-A fuel blends on combustion, emission and exergetic analysis using a micro-gas turbine engine. Fuel 2020;276:118104.
[22] Lopez Pintor D, Gentz G, Dec J. Mixture stratification for CA50 control of LTGC engines with reactivity-enhanced and non-additized gasoline. SAE 2021–01-0513 Technical Paper Series 2021. https://doi.org/10.4271/2021-01-0513.
[23] Yu L, Wang S, Wang W, Qiu Y, Qian Y, Mao Y, et al. Exploration of chemical composition effects on the autoignition of two commercial diesels: Rapid Compression Machine experiments and model simulation. Combustion and Flame 2019;204:204–19.
[24] Kang D, Kalaskar V, Kim D, Martz J, Violi A, Boehman A. Experimental study of autoignition characteristics of Jet-A surrogates and their validation in a motored engine and a constant-volume combustion chamber. Fuel 2016;184:565–80.
[25] Martin CD, Shepherd JE. Low temperature autoignition of jet A and surrogate jet fuel. Journal of Loss Prevention in the Process Industries 2021;71:104454.
[26] ASTM D7668-17, "Standard Test Method for Determination of Derived Cetane Number (DCN) of Diesel Fuel Oils—Ignition Delay and Combustion Delay Using a Constant Volume Combustion Chamber Method," *ASTM International*, West Conshohocken, PA, 2021.
[27] Cheng S, Kang D, Fridlyand A, Goldsborough SS, Saggese C, Wagnon S, et al. Autoignition behavior of gasoline/ethanol blends at engine-relevant conditions. Combustion and Flame 2020;216:369–84.
[28] Cheng S, Saggese C, Kang D, Goldsborough SS, Wagnon SW, Kukkadapu G, et al. Autoignition and preliminary heat release of gasoline surrogates and their blends with ethanol at engine-relevant conditions: Experiments and comprehensive kinetic modeling. Combustion and Flame 2021;228:57–77.
[29] Lawson R, Gururajan V, Movaghar A, Egolfopoulos FN. Autoignition of reacting mixtures at engine-relevant conditions using confined spherically expanding flames. Proceedings of the Combustion Institute 2021;38(2):2285–93.
[30] Farouk TI, Dietrich D, Dryer FL. Three stage cool flame droplet burning behavior of N-alkane droplets at elevated pressure conditions: Hot, warm and cool flame. Proceedings of the Combustion Institute 2019;37(3):3353–61.
[31] Heywood J. Internal Combustion Engine Fundamentals. New York: McGraw-Hill; 1988.
[32] Yehia OR, Reuter CB, Ju Y. Low-temperature multistage warm diffusion flames. Combustion and Flame 2018;195:63–74.
[33] Ju Y, Reuter CB, Yehia OR, Farouk TI, Won SH. Dynamics of cool flames. Progress in Energy and Combustion Science Aug. 2019;75(2019).
[34] Reuter CB, Lee M, Won SH, Ju Y. Study of the low-temperature reactivity of large N-alkanes through cool diffusion flame extinction. Combustion and Flame 2017;179:23–32.
[35] Reuter CB, Won SH, Ju Y. Experimental study of the dynamics and structure of self-sustaining premixed cool flames using a counterflow Burner. Combustion and Flame 2016;166:125–32.
[36] Soloiu V, Wiley JT, Gaubert R, Mothershed D, Carapia C, Smith RC, et al. Fischer-Tropsch coal-to-liquid fuel negative temperature coefficient region (NTC) and low-temperature heat release (LTHR) in a constant volume combustion chamber (CVCC). Energy 2020;198:117288.
[37] Colket M, Zeppieri S, Dai Z, Hautman D. "Fuel research at UTRC", *5th annual fuel research meeting multi-agency coordinating council for combustion research*, Livermore. CA: Sandia National Laboratories; 2012.
[38] Shiraishi T. A study of low temperature plasma-assisted gasoline HCCI combustion. SAE International Journal of Engines 2019;12(1):31–44.
[39] Jain A, Krishnasamy A, P. v,. Computational optimization of reactivity-controlled compression ignition combustion to achieve high efficiency and clean combustion. International Journal of Engine Research 2020;22(7):2213–32.
[40] Daly SR, Tran K, Niemeyer KE, Cannella WJ, Hagen CL. Predicting fuel low-temperature combustion performance using Fourier-transform infrared absorption spectra of neat hydrocarbons. Fuel 2019;242:343–4.
[41] Niemeyer KE, Daly S, Cannella W, Hagen C. Investigation of the LTC fuel performance index for oxygenated reference fuel blends. Fuel 2016.
[42] Lefebvre AH, Ballal DR. Gas turbine combustion alternative fuels and emissions. Boca Raton: Taylor & Francis; 2010.
[43] Soloiu V, Smith R, Weaver A, Grall D, Carapia C, Parker L, et al. Investigations of low-temperature heat release and negative temperature coefficient regions of iso-Paraffinic kerosene in a constant volume combustion chamber. In: ASME 2021 Internal Combustion Engine Division Fall Technical Conference; 2021. https://doi.org/10.1115/ICEF2021-68203.
[44] Khandelwal B, Wijecinghe CJ. Aviation fuels. 1st ed. London: Academic Press; 2021.
[45] de La Barbosa M, Cruz Garcia S, Ducruix BL, Lacas F. Control of combustion instabilities by local injection of hydrogen. Proceedings of the Combustion Institute 2007;31(2):3207–14.

[46] Nemitallah MA, Abdelhafez AA, Ali A, Mansir I, Habib MA. Frontiers in combustion techniques and burner designs for emissions control and CO_2 capture: A Review. International Journal of Energy Research 2019.
[47] J. R. Seume, N. Vortmeyer, W. Krause, J. Hermann, C.-C. Hantschk, P. Zangl, S. Gleis, D. Vortmeyer, and A. Orthmann, "Application of active combustion instability control to a heavy-duty gas turbine," ASME 1997 Turbo Asia Conference, 1997.
[48] Huang Y, Ratner A. Experimental investigation of thermoacoustic coupling for low-swirl lean premixed flames. Journal of Propulsion and Power 2009;25(2):365–73.
[49] Emadi M, Kaufman K, Burkhalter MW, Salameh T, Gentry T, Ratner A. Examination of thermo-acoustic instability in a low swirl burner. International Journal of Hydrogen Energy 2015;40(39):13594–603.
[50] Bahri B, Shahbakhti M, Kannan K, Aziz AA. Identification of ringing operation for low temperature combustion engines. Applied Energy 2016;171:142–52.
[51] Massey JA, Drallmeier JA. Identification of the dominant combustion characteristics on homogeneous charge compression ignition engine noise. International Journal of Engine Research 2014;16(4):518–30.
[52] Dernotte J, Dec JE, Ji C. Investigation of the sources of combustion noise in HCCI engines. SAE International Journal of Engines 2014;7(2):730–61.
[53] Dowling AP, Mahmoudi Y. Combustion noise. Proceedings of the Combustion Institute 2015;35(1):65–100.
[54] Wissink M, Wang Z, Splitter D, Shahlari A, Reitz RD. Investigation of pressure oscillation modes and audible noise in RCCI, HCCI, and CDC. SAE Technical Paper Series 2013.
[55] V. Soloiu, R. Smith, D. Grall, A. Knowles, C. Carapia, and C. Phillips, "Exploratory investigation of combustion and NVH signature of a drone jet engine fueled with IPK," *AIAA SciTech Forum*, Jan. 2020.
[56] Valentin Soloiu, Drake T. Grall, Marcel Ilie, Cesar Carapia, Richard C. Smith III, and Austin Brant, "Numerical And Experimental Analysis Of A Single Stage Drone Jet Engine" AIAA Propulsion and Energy Forum August 9-11, 2021, VIRTUAL EVENT AIAA Propulsion and Energy 2021 Forum, | http://arc.aiaa.org | DOI: 10.2514/6.2021-3488.
[57] Parr Instrument Company. 2021. 6772 Calorimetric Thermometer. Accessed 9 20, 2021. Cahttps://www.parrinst.com/products/oxygen-bomb-calorimeters/6772-calorimetric-thermometer/.
[58] Parr Instrument Company. N.d. Series 1341 Plain Jacket Oxygen Combustion calorimeters. Moline. Parr Instrument Company. 2014. Series 1341 Plain Jacket Oxygen Combustion Calorimeters. Moline. Accessed 9 20, 2021.
[59] Wan K, Manin J, Sim HS, Karathanassis I. Soot and PAH formation in high pressure spray pyrolysis of gasoline and diesel fuels. Combustion and Flame 2022;241:112084.
[60] Kalvakala KC, Pal P, Gonzalez JP, Kolodziej CP, Kukkadapu G, Wagnon S, et al. Numerical Analysis of soot emissions from gasoline-ethanol and gasoline-butanol 1 blends under gasoline compression ignition conditions. SSRN Electronic Journal 2022.
[61] Yousuffuddin S. Effect of combustion duration on the operating and performance characteristics of hydrogen-ethanol dual fueled engine: an experimental analysis. Int. J. Adv. Autom. Technol. 2017;1(1):36–45.
[62] Alhikami C-E, Wang W-C. A study of the spray ignition characteristics of hydro-processed renewable diesel, petroleum diesel, and biodiesel using a constant volume combustion chamber. Combustion and Flame 2021;223:55–64.
[63] "Laser diffraction," *Sympatec*. [Online]. Available: https://www.sympatec.com/en/particle-measurement/glossary/laser-diffraction/. [Accessed: 13-Mar-2022].
[64] Manigandan S, Gunasekar P, Poorchilamban S, Nithya S, Devipriya J, Vasanthkumar G. Effect of addition of hydrogen and TIO2 in gasoline engine in various exhaust gas recirculation ratio. International Journal of Hydrogen Energy 2019;44(21):11205–18.
[65] Zeng W, Sjöberg M, Reuss DL, Hu Z. High-speed PIV, Spray, combustion luminosity, and infrared fuel-vapor imaging for probing tumble-flow-induced asymmetry of gasoline distribution in a spray-guided stratified-charge Disi engine. Proceedings of the Combustion Institute 2017;36(3):3459–66.
[66] H. Kuszewshi "Physical and Chemical Properties of 1-Butanol-Diesel Fuel Blends" *Energy Fuels* 2018, 32, 11, 11619–11631 Publication Date: October 23, 2018, https://doi.org/10.1021/acs.energyfuels.8b02912.
[67] da Costa RB, Coronado CJR, Hernández JJ, Malaquias AC, Flores LF, de Carvalho JA. Experimental assessment of power generation using a compression ignition engine fueled by farnesane – a renewable diesel from sugarcane. Energy 2021;233:121187.
[68] PAC, "Cetane ID 510 Operating Manual," Petroleum Analyzer Company, 8001-00x-01E-C.
[69] Merkel AC, Ciccarelli G. Diesel spray ignition behind a reflected shock wave. Combustion and Flame 2020;217:237–47.
[70] J. I. Ryu, A. Motily, T. Lee, R. Scarcelli, S. Som, K. Kim, and C.-B. Kweon, "Ignition enhancement of F-24 jet fuel by a hot surface for aircraft propulsion systems," *AIAA Scitech 2020 Forum*, 2020.
[71] Goldsborough SS, Hochgreb S, Vanhove G, Wooldridge MS, Curran HJ, Sung C-J. Advances in rapid compression machine studies of low- and intermediate-temperature autoignition phenomena. Progress in Energy and Combustion Science 2017;63:1–78.
[72] Dafsari RA, Lee HJ, Han J, Park D-C, Lee J. Viscosity effect on the pressure swirl atomization of an alternative aviation fuel. Fuel 2019;240:179–91.
[73] Zettervall N, Fureby C, Nilsson EJK. A reduced chemical kinetic reaction mechanism for kerosene-air combustion. Fuel 2020;269:117446.
[74] Wang Z, Mani Sarathy S. Third O2 Addition Reactions Promote the Low-Temperature Auto-Ignition of N-Alkanes. *Combustion and Flame* 165 2016:364–72. https://doi.org/10.1016/j.combustflame.2015.12.020.
[75] Wang Z, Chen B, Moshammer K, Popolan-Vaida DM, Sioud S, Shankar VS, et al. N-heptane cool flame chemistry: Unraveling intermediate species measured in a stirred reactor and motored engine. Combustion and Flame 2018;187:199–216.
[76] Peters N, Paczko G, Seiser R, Seshadri K. Temperature cross-over and non-thermal runaway at two-stage ignition of n-Heptane. Combustion and Flame 2002;128(1–2):38–59.